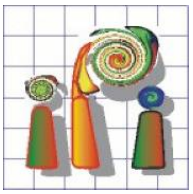

Institute für Photogrammetrie und Geoinformation

Diploma Thesis

Geometric Aspects of Large Size Digital Frame Cameras and Their Use for Photogrammetric Data Acquisition

---

Wu, Dun

Hannover, Germany, August 2007

Thesis supervisors

Dr. Karsten Jacobsen

Prof. Christian Heipke

Leibniz Universität Hannover

Support by Hansa Luftbild German Air Surveys

Institut für Photogrammetrie und GeoInformation
Leibniz Universität Hannover
Prof. Dr.-Ing. Christian Heipke

Nienburger Str. 1
D-30167 Hannover

Tel.: ++49-511/762-2485
Fax: ++49-511/762-2483
e-mail: jacobsen@ipi.uni-hannover.de
http://www.ipi.uni-hannover.de

Dr.-Ing. Karsten Jacobsen

Hannover, den 16.03.2007

Diplomaufgabe für
cand geod Wu, Dun

Geometrische Aspekte der großformatigen, flächenhaften digitalen Kameras und deren Berücksichtigung in der photogrammetrischen Auswertung

Geometric aspects of large size digital frame cameras and their use for photogrammetric data acquisition

Large size digital frame cameras are more and more replacing the traditional analogue film cameras for photogrammetric application. The large size digital frame cameras are based on a combination of smaller CCD-arrays. Some investigation showed geometric problems of the CCD-array merge to homogenous virtual images causing systematic images errors.

Based on the test blocks Gent, Rubi and Schwabach, taken by the Intergraph Z/I-Imaging DMC, and the block Istanbul, taken by the Microsoft Photogrammetry UltraCamD, the image geometry of the digital cameras has to be investigated and the geometric potential has to be analyzed. The analysis of the image geometry has to be made by bundle block adjustment with self calibration by additional parameters. The influence of the systematic image errors to the block configuration shall be investigated with and without combined bundle block adjustment with relative kinematic GPS-positioning if precise GPS-data of the projection centres are available.

The bundle block adjustment is able to determine and respect systematic image errors, but photogrammetric workstations usually cannot respect it for the model handling, leading to model deformations. The model deformations caused by the geometric problems shall be investigated.

Dr. Karsten Jacobsen

Erklärung

Hiermit erkläre ich, dass ich die vorliegende Arbeit selbständig verfasst und keine anderen, als die von mir angegebenen Quellen und Hilfsmittel benutzt sowie Zitate kenntlich gemacht habe.

Wu, Dun

Hannover, August, 2007

Acknowledgements

I would like to express my sincere gratitude to Dr. Jacobsen. Throughout my three years' study at the University of Hannover I have been impressed by the profundity of his knowledge and his amiability. Any academic accomplishments I have made during this period are as much a reflection of his efforts to motivate me as they are of anything else.

I must also thank for the support of Hansa Luftbild. My working at Hansa Luftbild led to important results for the diploma thesis. Special thanks go to Prof. Dr. Schroth and Dr. Li for their selfless help and invaluable feedback.

Finally, the deepest gratitude of all goes to my parents. Indeed, my entire education is the result of a thirst for knowledge that was sparked and encouraged by them. All that I am, and all that I ever will be, I owe to them.

Content

Chapter
1. Introduction

1.1 Develop of Digital Aerial Cameras

In the traditional way of airborne photogrammetric imaging a radical change in the last few years took place. Although still a large number of analogue film cameras are in use, with the advent and operational availability of digital aerial cameras a strong and powerful alternative to the standard manner of analogue imaging appeared.

The main advantages of digital aerial cameras over their analogue counterparts are the full digital workflow of image acquisition and processing:

- significant improved radiometric resolution,
- reproducible color information,
- cost savings for films,
- cost savings for film processing,
- cost savings for scanning
- immediate availability of the image data.
- together with the simultaneously acquired panchromatic and multi-spectral imagery

All these properties make the digital aerial camera readily applicable and thus more attractive for many applications, commonly for mapping, ortho-photos and DEM, even for 3D city modeling and updating, disaster monitoring and documentation, infrastructure mapping, precision farming etc.

Therefore, the development of digital aerial cameras has advanced significantly over the past 4-5 years. When talking about replacing analog large format film, only three commercially available digital cameras can be taken into account, namely Leica ADS40 [Leica Geosystem, 2000], DMC (Z/I Imaging, 2000), and UltraCamD and X (Vexcel, 2003). They are becoming standard for photogrammetric application.

1.2 The Elementary Principle of Digital Aerial Camera

The Two approaches to the design of digital aerial cameras are:

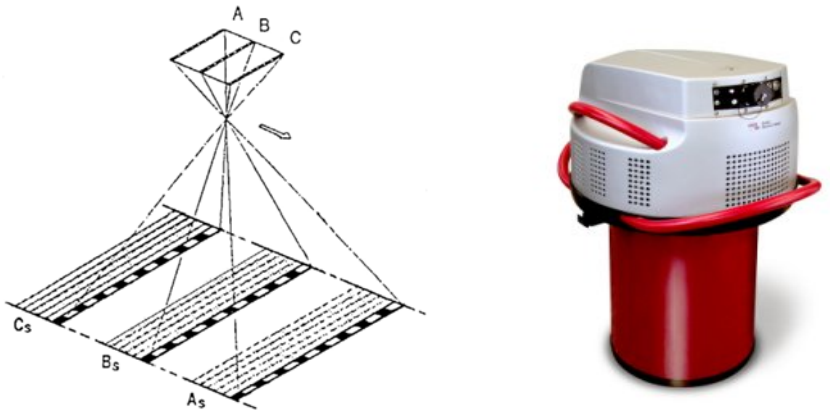

(a) (b)

Figure1.2-1: (a) Principle of the line scanner; (b) overview of the ASD40, Camera holding ten CCD lines

CCD-Scanner (figure1.2-1a): Systems based on CCD-line scanners (push-broom). CCD-line scanners acquire data by scanning the terrain with one or more CCD-lines as the aircraft moves over the terrain, in much the same manner as a broom sweeps a surface. The ADS40 incorporates three panchromatic CCD-lines, one looking forward, one looking vertically and one backwards to acquire three separate overlapping images of the terrain that can be used for 3D-application. Multi-spectral images at the same resolution are also acquired. An integrated GPS/IMU system is essential for this configuration for the determination of camera position and tilts, because the image acquisition is a continuous process and not frame based.

Figure 1.2-1b shows ADS40 system produced by Leica Geosystem, which was at first introduced as large format camera to the market in 2001.The ADS40 was designed based on CCD-lines, and comprises seven parallel linear sensors in the focal plane of a single lens system. Three panchromatic sensors scan the same ground area at different angles to acquire forward, nadir and backward scenes.

After the raw imagery and metadata are downloaded, the determination of exterior orientation parameters (based on position and attitude data from the integrated GPS/IMU system) and subsequent image rectification is possible. Consequently, stereo viewing in three combinations of two panchromatic bands, i.e. forward/nadir (F/N), forward/backward (F/B) and nadir/backward (N/B) is enabled. Nevertheless, at this stage the rectified data is insufficient for photogrammetric measurement because of the remaining y-parallax in the rectified images (present, for example, as result of

any misalignment between the IMU and camera axes and the datum between GPS/IMU and the ground control system), requiring photogrammetric bundle adjustment.

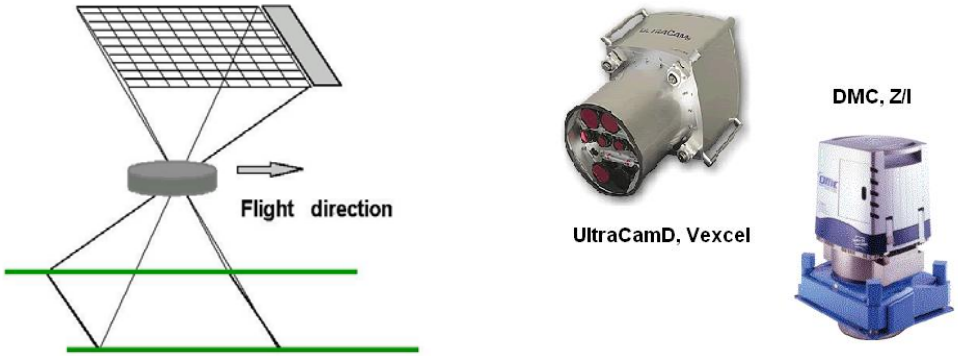

(a) (b)

Figure1.2-2: (a) Principle of CCD-Array Camera; (b) Digital Frame camera

CCD-Array: Systems based on CCD arrays: These systems may involve single area arrays (usually referred to small or medium resolution) or multiple arrays whose images are stitched together to form a larger frame image (referred to as high resolution). The formats of the images may not be square. These frame images can be processed using standard digital photogrammetric software. GPS/IMU system is not essential for its operation, but some components of such a system may be included as an option.

Figure 1.2-2b shows two large format digital frame cameras, the UltraCamD and the DMC respectively produced by Microsoft Photogrammetry (formerly Vexcel Imaging), Austria and Intergraph Z/I imaging, Germany. They are based on CCD array sensor technology and provide a very high interior geometric stability. According to their modular design, more than one individual camera module can be tied together, resulting in a large virtual image. The detailed information will be introduced in the following chapter.

The Leica ADS-40 has the disadvantage of scene accuracy dependency from the direct sensor orientation, based on relative kinematical GPS-positioning and inertial measurement units (IMU). The processing of CCD-line scanner images also requires special software for the photogrammetric workstation. For mapping purposes usually CCD-array cameras are preferred, while for large size ortho-image projects the CCD-line scanner has advantages [Jacobsen, 2007].

1.3 Motivation of the Diploma Thesis

The geometric accuracy and stability of complicated digital large-format sensors is an important issue. The performance of the sensors must be known and sensor calibration must be accurately determined in order to fully meet expectations.

In this thesis two type digital frame cameras, i.e. DMC and UltraCamD are investigated with the aim to analyze their geometric performance. What is the physical influence on the new digital camera systems, and how to improve the accuracy of images as well as to eliminate model and block deformation?

The results of bundle block adjustment provide an ideal base for estimating systematic image errors. The analyses of data sets mainly have been made with the Hannover photogrammetric program system BLUH. BLUH has its own set of additional parameters which is a combination of parameters with physical background completed by general parameters to allow a compensation of any general type of image deformation [Jacobsen, 2007]. BLUH is very flexible to handle special parameters for different type of cameras, in this thesis the special parameters for DMC and UltraCamD are introduced in the following chapter.

Analysis in image as well as in object space, the two different ways are introduced in the thesis. The first way tries to show systematic image errors of the camera system, the σ_0 – the accuracy of the image coordinates and averaged residuals of image observations describe the systematic image errors properly with simultaneous self-calibration using additional parameters. Under the second way, the results of bundle block adjustment without or with self-calibration can indicate the systematic influence on the geometric accuracy in the object space, especially shown at independent check points. The model deformation caused by systematic image errors is also a big problem for stereo plotting and the generation of DEM. Therefore the different functional models are tested concerning their efficiency to compensate image errors and even to eliminate the model and block deformation.

Some data has been also dealt with photogrammetric program Match-AT, Inpho, which shows some different results than BLUH. They are discussed in the following chapter.

Chapter
2. General Information

2.1 Digital Mapping Camera (DMC) of Z/I Imaging

Intergraph's Z/I Imaging® DMC® (Digital Mapping Camera) is a digital camera system. It is based on CCD-array principle. Ideally, a single chip with an appropriate size and resolution should be used to transfer the photogrammetric capabilities of the analogue film cameras like RMK-Top to the digital technique. However, for the technological and economical reasons, it is not possible to choose the ideal solution which would be one individual, large CCD chip in the size of a silicon pizza. In the DMC system, four panchromatic sub-camera are tied together, resulting in a large virtual image, it provides a very high geometric stability.

2.1.1 DMC Camera

The DMC Camera unit (Figure 2.1.1-1a) consist eight internal sensors: 4 panchromatic sensors and 4 multi-spectral sensors integrated in the stabilized T-AS platform (Figure 2.1.1-1b). The multi-spectral sensors have 3k x 2k pixels, with one sensor capturing red data, one capturing the blue data, one capturing the green data, and one capturing near-infrared data. The four panchromatic sensors each capture one image of a particular area (7k × 4k pixels each), which slightly overlap one another and are used to produce one large mosaiked virtual image having 7680 × 13824 pixels. All sensors have a radiometric dynamic range of 12 bits. From the image data captured by the camera, there is a variety of output options using the post-processing software.

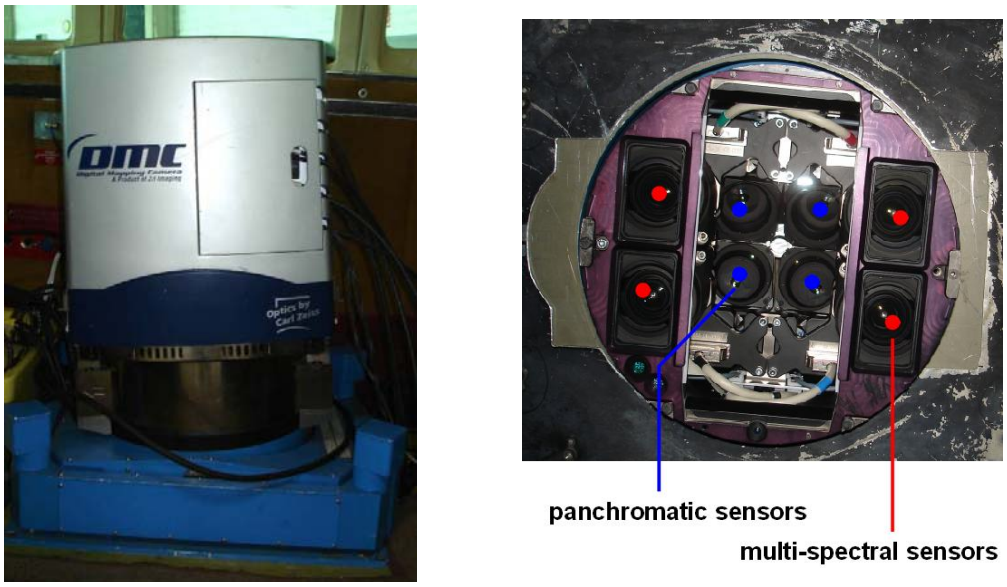

(a) (b)

Figure 2.1.1-1: (a) DMC Camera unit; (b) Mounting of the individual camera heads inside the DMC cone. [photo by Wu at Hansa Luftbild]

Optical Concept

The centerpiece of the system is the camera head and the CCD Matrix sensors as key element. For technological and economical reasons, it is not possible to choose the ideal solution which would be one individual, large-area very expensive CCD chips with the size of a "silicon pizza", similar to existing film formats. However, for the image recording procedure it is important to have ground coverage with one shot as wide as possible. This is provided by parallel operation of several compact camera heads, where each CCD has its own lens. The modules are directed to the scene at slightly displaced field angles [Tang et al., 2000].

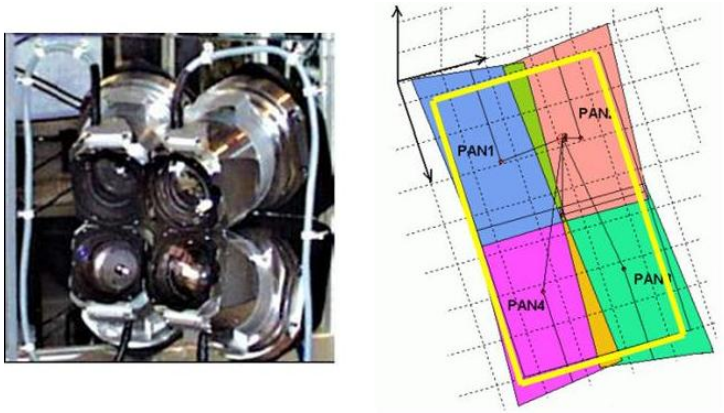

(a) (b)

Figure 2.1.1-2: (a) Configuration of panchromatic camera heads; (b) Footprint of 4 pan-images projected into the virtual image (yellow area) [Madani, et al., 2004]

Figure 2.1.1-2a shows the arrangement of the 4 panchromatic camera heads with convergent angles integrated in the stabilized platform and figure 2.1.1-2b the virtual image composed by the four camera heads. The virtual image has 13,824 pixels across track and 7,680 pixels along track. The camera system field of view is 69.3° × 42°.

The image recording must be performed parallel; it means that the exposure of all cameras takes place synchronously at exactly the same instant. The mounting of the panchromatic camera heads is modeled by four sets of interior orientation parameters, three position parameters (*x, y, z*) of projection centers and three orientation angles (φ, ω, κ) for the tilting of the heads inside the DMC cone. The position of the panchromatic camera projection centers within the DMC cone are precisely known, but the exact mounting angles of the four heads are not available with the required accuracy. Precise determination of the angles is absolutely necessary; otherwise it's not possible to merge the resulting individual images into one large high-resolution virtual image seamlessly [Dörstel et al., 2002]. The determination of the mounting angles is therefore essential for performance of the DMC and is called "platform calibration", which will be explained in detail (*chapter 2.1.2 DMC Processing*).

CCD-Sensors

Because of the better signal to noise relation, CCD- and not CMOS-sensors are used. The CCDs of DMC are full frame sensors with high optical fill factor and sensitivity and are manufactured by Philips in Eindhoven. Pixel size is 12 µm ×12µm, offering a high linear dynamic range >12 bit. The architecture of the CCDs offers 4 readout registers on every corner of the chip. This provides high readout rates, which is important for a good repetition rate of the system a mage every 2 seconds. The front end electronics, generating the CCD control, timing signals and the digital signal readout circuits are placed directly behind the CCD housing in order to ensure low noise performance of the system. Digitizing of the CCD signals is done with 12 bit resolution. [Hinz et al., 2001]

Figure 2.1.1-3 shows the 7k × 4k CCD-chip and the front end electronics. The high resolution CCD-chip is packaged into a customized Al203 housing. Special care has been taken in the development of this housing to ensure very high stability of the geometry during pressure (flying height) and temperature variations.

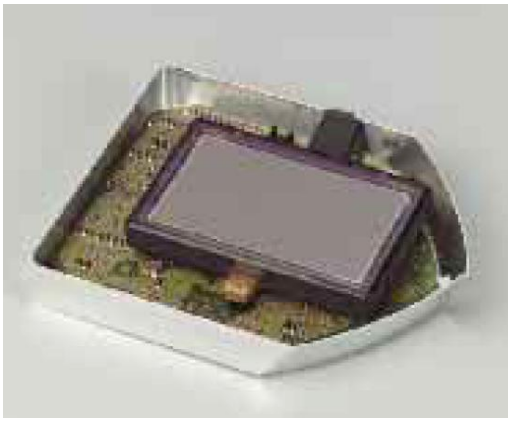

Figure 2.1.1-3: 7k X 4k CCD-chip package and front end electronics. [Hinz et al., 2001]

2.1.2 DMC Processing

During flight mission the raw data, which contain all images of the particular panchromatic and multi-spectral sensors, are captured and stored on board. After landing of the aircraft the raw data are subsequently transferred to the DMC post-processing station, at which image composites are generated. The complete workflow including flight project planning and image data capturing is illustrated in the following table 2.1.2-1. This is an example of a typical project from start to end.

The primary products of DMC post-processing are the high resolution panchromatic and multi-spectral virtual image, generated by means of 4 panchromatic sub-images and 4 multi-spectral images, which is introduced detailed in the following paragraph.

Processing Site	Processing Step	Details In Step
Office	Pre-Processing	Mission Planning
Airplane	Photo Flight	Navigation and Flight Management System Camera Software Control Module Quick view (In-flight Quality Check)
Office	Post-Processing	Connection of Flight Data Storage (FDS) or Copy Station disks **Post-Processing** ● Radiometric correction ● Geometric correction ● Mosaicking (generate virtual images) ● Color image generation Data distribution
Office	Data Exploitation	Data processing via photogrammetric/GIS tools

Table 2.1.2-1: workflow of DMC processing

DMC Post-Processing Overview

At first, the geometric and radiometric calibration for single camera head is determined in laboratory, which is done once during manufacturing the DMC. The information generated during this procedure will then be used by the post-processing to mosaic the high resolution images and the color channel images into one high resolution RGB or infrared false color virtual image.

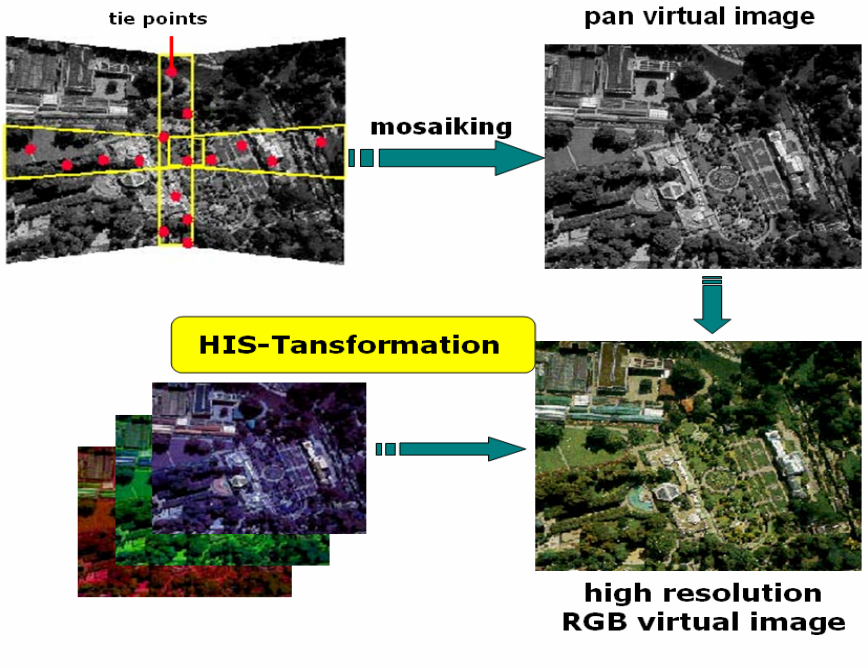

Figure 2.1.2-1: DMC post-processing

The following tasks must be performed in the post-processing software (*see figure 2.1.2-1*) for every image exposure [Dörstel et al., 2002]:

- Extraction of tie points in the overlapping areas of the four panchromatic images using matching techniques. The laboratory calibrations of the single camera heads are applied to generate corrected image coordinates of the tie points.
- Determination of the mounting angles of the panchromatic heads by a bundle block adjustment technique - ***platform calibration***
- Computation of transformation parameters using the four sets of exterior orientation parameters to map from the single images to the virtual image.
- Projection of the single panchromatic images to the high resolution virtual image using the computed transformation parameters.
- Extraction of tie points between the high resolution virtual image and the

four color channel images.

- Computation of transformation parameters using the extracted tie point image coordinates to map from the color channel images to the virtual image.
- Mapping of the color channel images to the virtual image using the computed transformation parameters (Color fusion).
- Generation of overviews of the high resolution color image and writing the output to disk.

Approach of Platform Calibration

The following data serves as input for the platform calibration:

- four panchromatic images;
- lens distortion information for the four panchromatic images;
- precise knowledge of the position of the panchromatic camera projection centers within the DMC cone;
- approximations of the interior orientation angles (tilting of the camera heads);
- approximations of the focal lengths of the panchromatic camera heads;

In the first step, tie points in the four overlapping regions are extracted. This is done by mapping a point grid from a master image via the approximated orientation parameters to all three slave images. The resulting matching candidates will then be refined by least squares matching techniques. The image coordinates of the tie points are corrected for lens distortion and serve as main input to the bundle block adjustment module. An example of extracted tie points is shown in Figure 2.1.2-1, the total number of tie points can be selected and optimized for computation speed. However, investigations show that very good results can be already achieved by using only 30-50 well distributed points. [Dörstel et al., 2002]

The next step in performing the platform calibration is the bundle block adjustment module. This module is based on the well known software package BLUH [Jacobsen，1998]. It solves for the four sets of orientation angles and for three focal lengths. Unknowns of the common bundle adjustment of the four panchromatic images are attitude data for three images in relation to a reference image, 3 focal length and a special additional parameter controlling the projection centre offset in relation to the flying height above ground, while the location of the precisely known projection centers are used for the determination of the other unknowns. [Dörstel et al., 2002]

Mosaicking Process

The mosaicking process takes the results of the platform calibration and combines the four panchromatic images into the virtual DMC image. The position of the projection centers of the panchromatic cameras is well known, the tilting angles as well as the focal lengths of the cameras are adjusted by the platform calibration. To project each pixel from the panchromatic camera to the virtual DMC image, it's necessary to define the properties of the virtual camera. The virtual projection center is per definition located in the center of the four real projection centers, the optical axis of the virtual camera is defined as the mean optical axis of the four panchromatic optical axes. The focal length can be selected as desired, but was set to 120.000 mm for minimization of scale differences. All this information allows the projection of each position in the real image to the virtual image using the well-known co-linearity equations. [Dörstel et al., 2002]

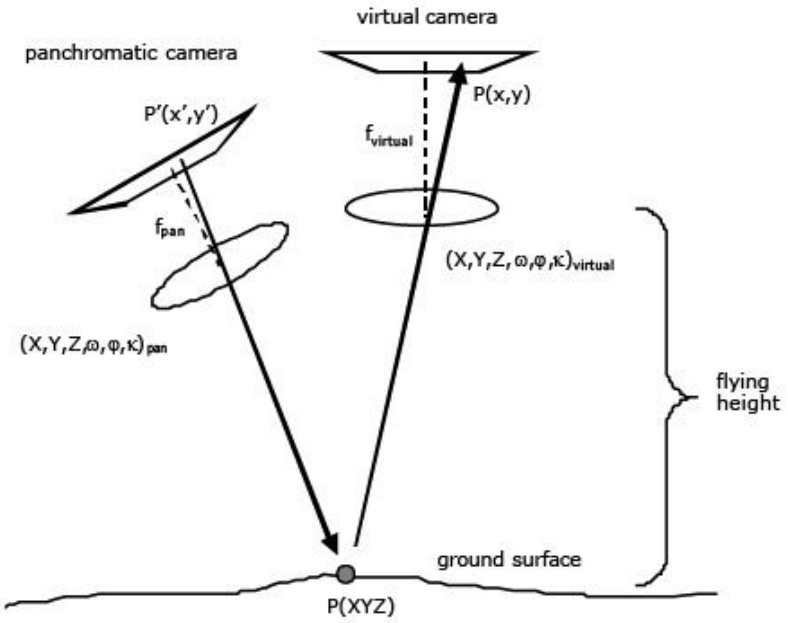

Figure 2.1.2-2: Projecting an image point from the real panchromatic image to the virtual DMC image using project centers, focal lengths, image coordinates and the flying height. [Dörstel et al., 2002]

For performance reasons, the method of projection described above is only applied to raster points forming a grid on the panchromatic single images. These grid points are transferred rigorously (including lens distortion information), and the resulting image coordinates gives together with the input values four sets of identical points, one for each panchromatic image. Following by this, four sets of rational function coefficients are fitted to the identical points using least squares techniques. If the desired level of accuracy is not reached, more grid points are generated, until the maximum residual is less than a certain threshold. By using the rational function coefficients, a performance optimized software maps the single images directly into the virtual image tile by tile. During this mapping, a blending algorithm ensures a smooth

transition between the four images in the virtual DMC image.

Figure 2.1.2-3: results of the mosaiking process. [Dörstel et al., 2002]

Figure 2.1.2-3 shows that the center of the virtual DMC image is located in the center of the roof. The tie point extraction, the lens distortion correction and the rectification has been done. The four edges of the panchromatic images fit together very well as it can be seen in the left image. After applying a blending algorithm, even the radiometric differences between the images are removed (right image).

2.2 Digital Aerial Camera (UltraCam$_D$) of Microsoft Photogrammetry

Microsoft Photogrammetries (formerly Vexcel Imaging) UltraCam$_D$ Digital Aerial Camera System delivers large format aerial imagery. It is based on CCD-array principle as the DMC.

The concept of the UltraCamD resembles DMC, and is to combine image data of several CCD sensors and several optical cones to one big virtual image that satisfies a central perspective. Four cones looking parallel to the ground holding nine CCD sensors, which collect the panchromatic data. These cones are aligned behind one another along flight direction and have the same field of view. The main idea is to expose the different optical cones at the exact same spot using the kinematics of the airplane. This synchronized exposure is called synoptic due to [Leberl et al., 2003] and guarantees that all panchromatic images have the same projection center (figure-2.2-1b). True color RGB and NIR images are collected by four separated cones, holding four CCD sensors, where the focal length is chosen such, that color and panchromatic images have the same field-of-view. High resolution color RGB and false color CIR images are produced by fusing the information of low-resolution color and high-resolution panchromatic information.

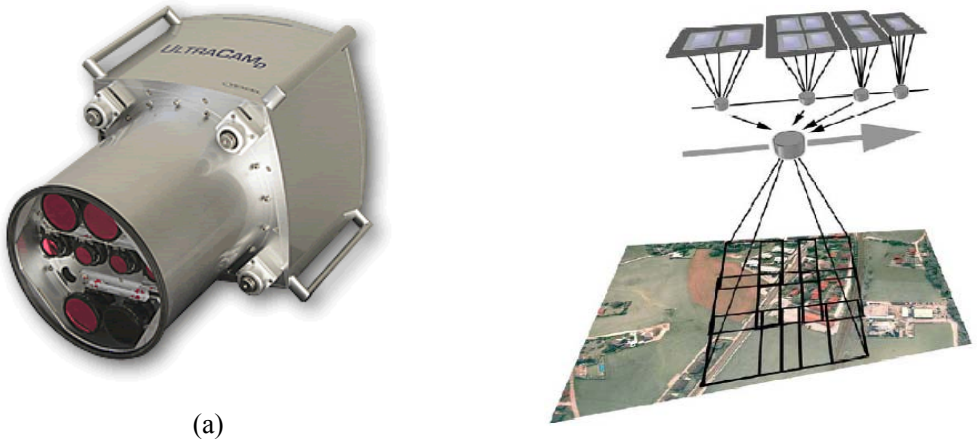

(a) (b)

Figure 2.2-1: (a) UltraCamD Camera Unit; (b) Principle of spot-synchronized exposure of the four panchromatic cones

2.2.1 UltraCam$_D$ Camera Unit

Figure 2.2-1a shows that the camera unit consists of a set of eight optical cones holding a total of 13 CCD arrays to assemble a large format image in RGB and false color NIR. The four cones in the center collect data for the high-resolution panchromatic image while four cones beside collect color information. The panchromatic part of the camera combines a set of 9 medium format CCD sensors into a large format panchromatic image at a size of 11500×7500 pixels. The multi-spectral channels are supported by four additional CCD sensors, i.e. red, green blue and near infrared.

2.2.2 Calibration of UltraCamD Cones

The UltraCamD creates a large format image by means of four optical so-called "cones". The geometric performance of the camera is defined by the so-called "master cone", which consists of four area-based CCD-arrays in the corners of its field-of-view. The four CCDs define the large format panchromatic image of the UltraCamD, while the gaps between these four sensors are filled by the other three panchromatic cones, which produce five sub-images with two or one CCD arrays per cone. This principle is sketched in figure 2.2.2-1a & b: The four panchromatic ones holding nine CCD sensors are aligned in one line along flight direction. The transformation between cones is determined by the calibration, for each frame, by tie point matching. The merging of the individual image segments into a full-format image was denoted by "stitching". The four multi-spectral cones on the both sides are collection RGB and NIR images.

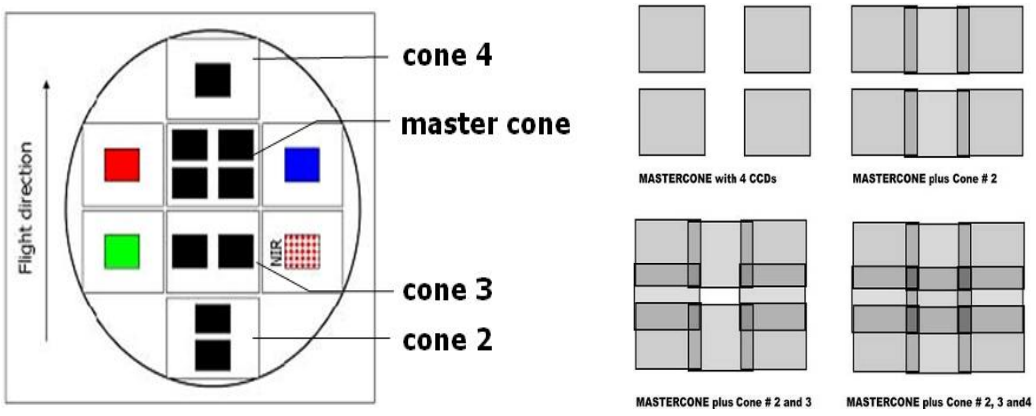

(a) (b)

Figure 2.2.2-1: (a) the arrangements of the CCD sensors of UltraCam$_D$; (b) The backplanes of four cones of the panchromatic channel produce a set of 9 sub-images. These get sequentially grouped. The master cone on the upper left with its four CCDs defines the geometry of the large format image.

Figure 2.2.2-2-a shows the 3D calibration target. Its dimensions are 3.3 × 2.4m^2 with a depth of 2.4m. Three fixed camera stations are available. The target consists of 240 well defined points, surveyed at an accuracy of ±50µm in X, Y and Z. The points are fixed on the rear wall, the sidewalls, the ceiling and the floor. The data capture is done from the three camera stations, where tilting and rotating the camera leads to a set of images from each station. The principle of capturing is visualized in figure 2.2.2-2 (b). A set of 84 images is taken from three image stations by rotating and tilting the camera. The full set of image coordinates measured consists typically of about 14000 positions within the set of panchromatic cones of the UltraCamD. The precision of the target detection algorithm was investigated and a deviation of about ±1.3µm (i.e. 0.14 pixel) has been observed [Kröpfl et al., 2004a].

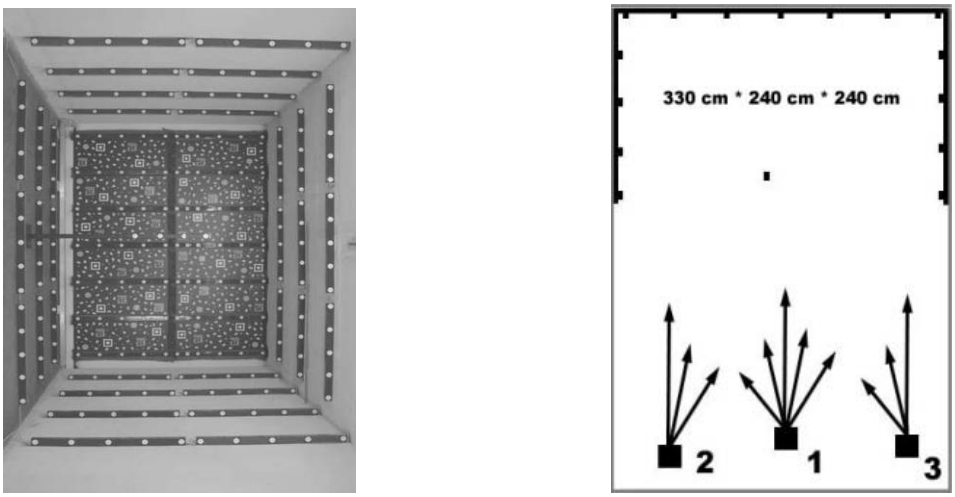

(a) (b)

Figure 2.2.2-2: (a) Calibration test field in the basement of Vexcel Imaging Austria office building. The test field consists of 240 precisely control points; (b) Three Camera positions are established

The adjustment of all image coordinate measurements and the estimation of camera parameters are performed with the software package BINGO [Kruck, 1984], and the entire adjustment procedure is fourfold:

- Calculation of the initial solution of camera parameters including parameters of CCD position, focal length, principal point coordinates and lens distortion.
- Transformation of image coordinates (the measurements) to clear CCD position parameters. This step needs several iterations in order to avoid any eccentricity of the radial distortion parameters of the lens cone.
- Description of remaining displacements in the image plane and description of the displacements by means of a lookup table.
- Estimation of transform parameters between cones in order to guide the post-processing (stitching) of the large format panchromatic image.

Calibration Report

Image Format	long track	67.5mm	7500 pixel
	cross track	103.5mm	11500 pixel
Image Extent		(-33.75, -51.75)mm	(33.75, 51.75)mm
Pixel Size		9.000µm*9.000µm	
Focal Length	ck	101.400mm	± 0.002mm
Principal Point	X_ppa	0.000 mm	± 0.002mm
(Level 2)	Y_ppa	0.000 mm	± 0.002mm
Lens Distortion	Remaining Distortion less than 0.002mm		

Table 2.2.2-1: large format panchromatic output image

Image Format	long track	67.5mm	2400 pixel
	cross track	103.5mm	3680 pixel
Image Extent		(-33.75, -51.75)mm	(33.75, 51.75)mm
Pixel Size		28.125µm*28.125µm	
Focal Length	ck	101.400mm	
Principal Point	X_ppa	0.000 mm	± 0.002mm
(Level 2)	Y_ppa	0.000 mm	± 0.002mm
Lens Distortion	Remaining Distortion less than 0.002mm		

Table 2.2.2-2: medium format multi-spectral output image

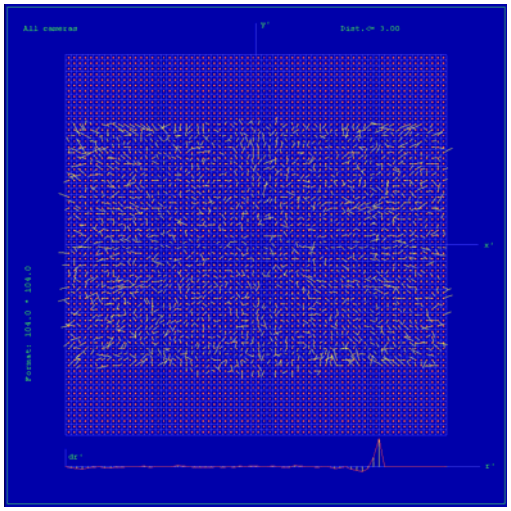

Figure 2.2.2-3: residual error diagram of full pan image, residual error (RMS) =0.81µm

2.2.3 Stitching the panchromatic sub-images

The camera delivers 13 raw CCD images per exposure. Out of them high-resolution color and false color images are generated. The challenge of computer vision is the generation of the panchromatic image by means of image stitching and the registration of the multi-spectral channels to the stitched image. These registered color channels are then fused with the large panchromatic data to create a large format color image.

The workflow of stitching the large format is as follows:

After a process of mature deliberation the strategy for the special case of the UltraCam$_D$ is as follows: As all cones are geometrically calibrated with an accuracy of at least 2µm RMSE (which is equivalent to 2/9 pixel, since the physical pixel size of the used CCD is 9µm), each of the three slave cones has to be inserted into the rigid master cone. A geometric image accuracy of 2µm is named in [Vexcel Imaging Austria, 2003]. To be able to align the slave cones to the master cone, homologous points have to be extracted in the overlapping areas. Figures 2.2.3-1a & b show the concept of matching slave cone number 1 to the master cone. Basically the four overlaps are used to determine the geometric correspondence.

The initial solution for the geometric alignment of the single images is known from calibration, therefore approximations for the overlapping regions are known. Since the cone, holding the central image, only intersects with the master cone at the corners, this image is matched to the slave cones 1 and 2, when the alignments to the master cone are already known. These homologous points are then transformed to the master cone's coordinate system, so that the geometric alignment can be estimated for the central sensor too.

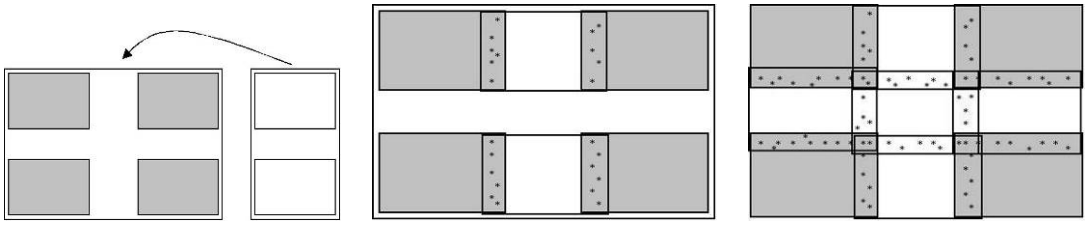

(a) (b) (c)

Figure 2.2.3-1: Stitching of the panchromatic UltraCamD image. (a) A slave cone is matched into the rigid master cone. (b) The geometric correspondence is established via homologous points (tie points). (c) All three cones, holding five images, are matched to the master cone.

Consequently, the homologous points for the twelve overlaps (*see figure 2.2.3-1c*) are extracted by defining points of interest in the overlap regions and reallocate them by

image matching in the second overlap.

For point of interest detection algorithm of Tomasi using structure tensor is used. The calculation of the corner response function defined by Tomasi is computationally not very time consuming and gives similar results as the function defined by Förstner.

Chapter
3. Simultaneous Calibration

3.1 Introduction

Using DMC und UltraCamD to create large size high resolution digital aerial images, several CCD sensors have to be combined to one virtual image, because of limited resolution of commercially available CCD sensor elements. This diploma thesis does not touch the manufacturer calibration of digital cameras. It's known that the laboratory calibration checks and corrects beside the geometric calibration also the radiometry of sensors. Despite of high efforts in labor calibration, systematic image errors are found in practical applications, showing clearly different effects of rotations, scaling and/or displacements for every CCD sensor element. As known from analog aerial survey film cameras, a simultaneous calibration has to be done, because of different environmental conditions between laboratory and under flight conditions.

The simultaneous calibration i.e. self-calibration with additional parameters is introduced in this thesis, which is able to determine geometric discrepancies between the mathematical model of perspective images and the real image geometry, this difference is called "systematic image errors" even if it is an error of the mathematic model [Jacobsen, 1998]. The parameter models of self-calibration are introduced in this diploma thesis, which are adapted to the special geometry of new digital survey cameras.

3.2 Potential Error Sources and Influences

Several error sources, which can be responsible for the appearance of the systematic image errors, are discussed in the next sections. These effects contain both errors appearing at digital cameras in general and especially at the DMC because of its special design and mapping concept. The discussion comprises the origin of the errors and their effect on the images coordinates.

3.2.1 Lens Distortion

Because components of cameras can be manufactured only with certain production accuracy, objects aren't reproduced strictly in the image plane like they should due to the theory of central perspective. This remaining effect is called lens distortion and can appear at every camera heads of DMC or UltraCam$_D$. A distinction is drawn between different forms of distortion such as radial, tangential, in-plane- and out-of-plane distortion.

Radial symmetric lens distortion (*figure 3.2.1-1*) emerges from manufacturing errors of the lens system and thermal influences under flight condition. It causes radial symmetric errors in the image point measurements. In addition asymmetric radial distortions may appear. Both types of radial distortion are the result of imperfections in the grinding of the camera lenses and the flight conditions. Symmetric radial distortion can change in sign and magnitude depending on the radial distance from the centre of the image. Positive radial distortion causes points to be located closer to the centre of the image than they otherwise would be. Corresponding negative distortion causes points to be imaged farther from the centre. Both types of distortion are shown in figure 3.2.1-1.

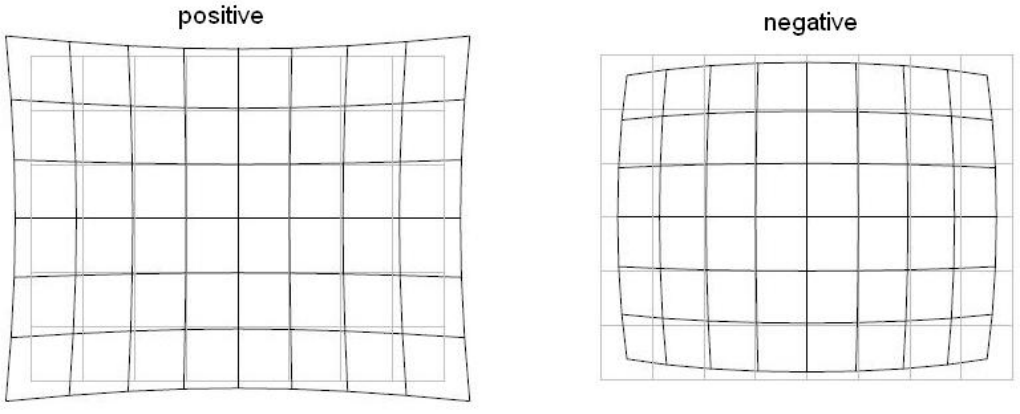

Figure 3.2.1-1: radial symmetric distortion - (a) pincushion distortion; (b) barrel distortion

The radial symmetric distortion can be described by an odd-powered polynomial function of the radial distance:

$$\delta r = k_0 r + k_1 r^3 + k_2 r^5 + k_3 r^7 + \ldots \qquad (3.2.1\text{-}1)$$

In Equation (3.2.1-1), δr is the error resulting from the radial distortion, the k_i terms are the coefficients of radial distortion, and r is the radial distance from the principal point of best symmetry. The latter is given by

$$r = \sqrt{x'^2 + y'^2} \qquad (3.2.1\text{-}2)$$

where *x'* and *y'* are the distances from the principal point of best symmetry, calculated as $x' = x\text{-}x_{pps}$ and $y' = y\text{-}y_{pps}$, respectively.

Tangential distortion (*figure 3.2.1-2*) is caused by the misalignment of the axes of the individual lenses along the common axis, and by the misalignment of the normal from the image plane with the camera's optical axis.

The model that is universally accepted for describing tangential distortions is formulated by Brown (1966). When higher order terms are ignored, the correction equations due to this model are

$$\begin{aligned} \delta x_d &= (r^2 + 2x'^2) \cdot P_1 + 2x'y' \cdot P_2 \\ \delta y_d &= 2x'y' \cdot P_1 + (r^2 + 2y'^2) \cdot P_2 \end{aligned} \qquad (3.2.1\text{-}3)$$

where p_1 and p_2 are the coefficients of tangential distortion, and *r*, *x'* and *y'* are as were given previously. This model is often referred as the Conrady-Brown model.

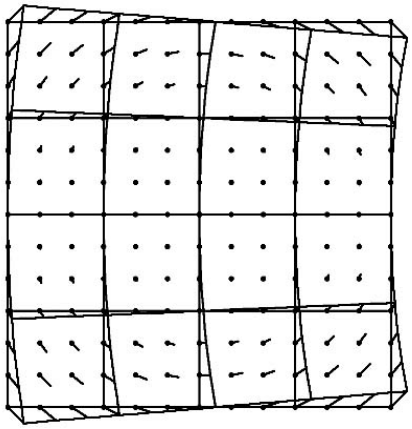

Figure 3.2.1-2: tangential distortion

The systematic image errors of analog film cameras are strongly influenced by the not-plane location of the film. CCD-arrays from the beginning have a very flat surface, but the surface may be deformed by temperature influences in a very regular manner. This may lead to effects like radial symmetric distortion, but a radial symmetric distortion may be caused also by a vertical temperature gradient in the lens system.

3.2.2 Change of Focal Length and Principal Point

The interior orientation of cameras can change because of vibrations of the aircraft or temperature influence. A changing of the principle point (x_0, y_0) results in a translation in x- or in y- image coordinates at the affected camera head. This effect is partly compensated during the post-processing in the bundle adjustment as a translation of camera heads is strongly correlated with the three orientation angles of the several camera heads. A shift can be compensated by approximating appropriate orientation angles. A changing of the principal distance corresponds to a scale change of the x- and y- image coordinates of the affected head. A change of the principal distance of all DMC sub-cameras by the same size causes systematic image errors corresponding to the special additional parameter 78 of BLUH (*see fig. 3.2.2-1*).

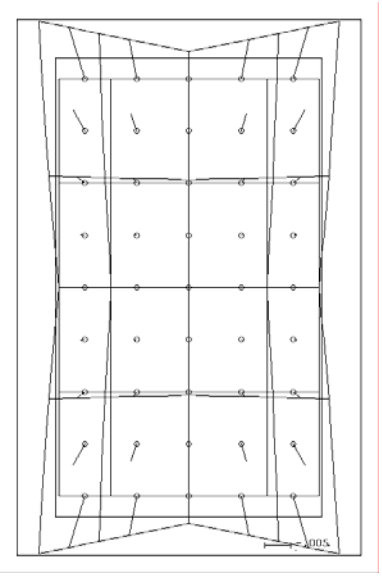

Figure 3.2.2-1: common influence of all DMC sub-images caused by the same change of the focal length of the sub-cameras

3.2.3 Geometry of sensor elements

As CCD sensors are built with an accuracy that is depending on precision of manufacturing, errors can appear, if the high expectations concerning geometric accuracy that are set in photogrammetry aren't fulfilled. Fabricating of CCD sensors to 0.3µm to 0.5µm design rules has been already standard in the year 1996 due to [Shortis & Beyer, 1996]. These design rules lead to possible systematic effects in the range of 0.2µm at a pixel size of 12um or 0.017 pixels.

These values shall be seen just as a benchmark as technology concerning CCD sensors has developed very fast in the last few years. For this reason it can be assumed that manufacturing precision and precision of measurement is much more accurate now than it has been ten years ago. However an insufficient geometric accuracy shows up for instance in deformed sensor elements or their irregular arrangement in a grid. These effects can be seen as constant over time and have a direct influence to the image coordinates.

These effects don't show up identically over the whole image plane, but differ randomly in shape and magnitude. Hence x- and y- image coordinates are influenced randomly depending on their position in the image plane.

3.2.4 Influence of FMC (TDI-shift)

The time delayed integration (TDI) shift is comparable to the forward motion compensation (FMC) used by analogue film cameras. The TDI mechanism allows the shift of the image in the focal plane depending upon the flying height and the aircraft speed. Under special conditions (e.g. very long exposure times), this shift can be about several dozens of the TDI shift to the geometry of the virtual DMC mosaicked image. Because of the inclined sub-camera arrangement the TDI-shift is limited usually to approximately 20 pixels, but theoretical investigations showed, that even a shift by 200 pixels is causing only discrepancies in the range of 1µm. This clearly indicates that a shifting of the image points due to the TDI mechanism has absolutely no effect to the mosaicked virtual DMC image; it's fully compensated by the adjusted orientation. [Dörstel et al, 2002]

3.2.5 Imprecise Synchronization of the Particular Camera Heads

If the four panchromatic raw images aren't exposed exactly at the same instant because of imprecise synchronization, image coordinates in the affected images are misaligned. This error affects mainly image coordinates in x. It is partly compensated during bundle adjustment in DMC post-processing as orientation angles are determined for every exposure of every single head. As a following the affected angle then gets a value that is higher or lower concerning the correct angle. It can be detected hardly as this angle has got the wrong value constantly for the whole block.

3.2.6 Eccentricity of Projection Centers

Because of approximating the strict solution at DMC post-processing step mosaicking with applying a plane instead of a DTM, image displacements arise in the virtual image, if the terrain is not flat. This is clarified in figure 3.2.7-1.

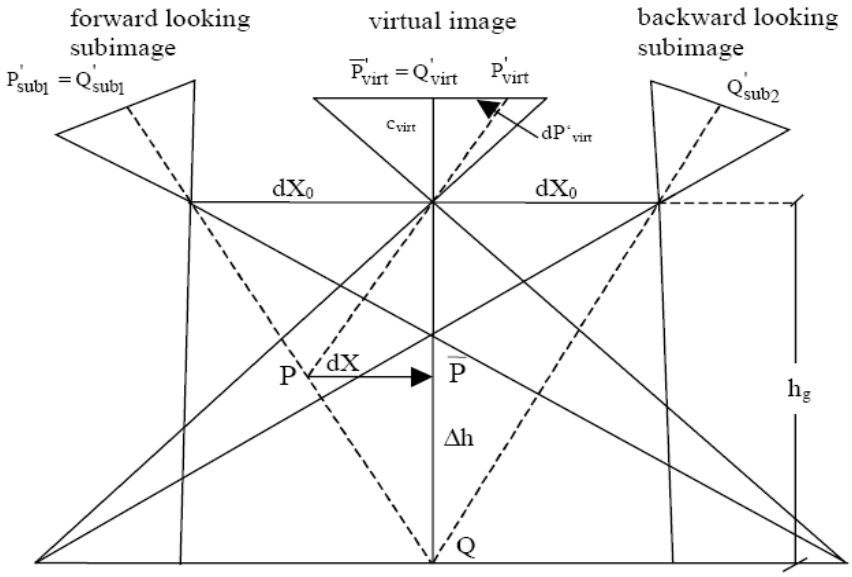

Figure 3.2.7-1: Geometric relations of the DMC in flight direction [Tang et al., 2000]

In figure 3.2.7-1 two sub-image planes are shown together with the one of the virtual image. With reference to this figure we first select a flying height. The point *Q* is located at the reference plane, so for this case the geometric mismatch is zero. If a point P is placed in a height Δh over the approximated plane, this causes a mismatch of the sub-images by dX in the virtual image.

The displacement in object space in the direction X and Y and the corresponding influence to the mismatch in x- and y-image coordinates can be calculated with the formulas of [Tang et al., 2000]:

$$\delta x' = \frac{c_{virt}}{h_g - \Delta h} dX = \frac{c_{virt}}{h_g} \cdot \frac{\Delta h / h_g}{(1 - \Delta h / h_g)} dX_0 \qquad (3.2.7\text{-}1)$$

$$\delta y' = \frac{c_{virt}}{h_g} \cdot \frac{\Delta h / h_g}{(1 - \Delta h / h_g)} dY_0 \qquad (3.2.7\text{-}2)$$

Here c_{virt} is the virtual focal length, h_g the flying height, Δh the difference between the reference plane and the earth's surface and δy' and δx' are the mismatch of the sub-images. As it can be seen in preceding formula, the magnitude of displacements depends especially on the ration $\Delta h/h_g$ and is decreasing with increasing flying height hg and increasing terrain height variation. Because of the larger offset of the

projection centers in the y- than in the x-direction, the effect is also larger in the y-image coordinate. The approximate image displacement in x- and y-image coordinates can be seen in following figure.

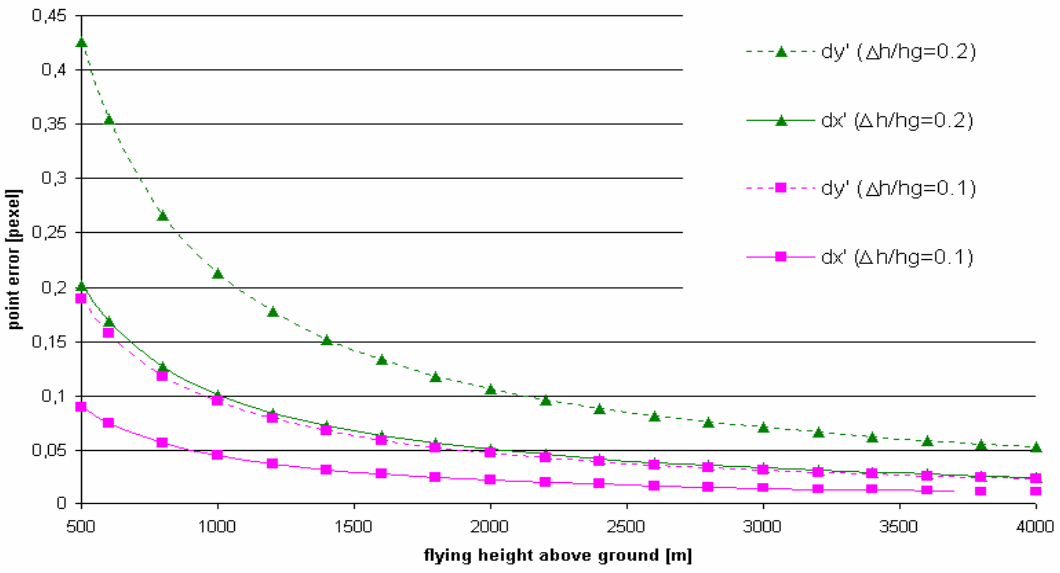

Figure 3.2.7-2: mismatch in *dx'* and *dy'* as a function of h_g and $\Delta h/h_g$ caused by the projection center offset. [Tang et al., 2000]

Due to preceding figure it is obvious that a block with low flying altitude is more affected. The blocks with a high flying altitude aren't affected to this extent. As can be seen influence is decreasing with increasing flying height. Influence for both blocks should be below 0.05 pixels.

Figure 3.2.7-2 shows the mismatch caused by the ratio of $\Delta h/h_g$ for different flying heights. As it can be seen, the dx' and dy' decrease with increasing flying height, and its values are not very large even for small values of hg. For the Y-component it could reach up to 0.43 pixel for a flying height of 500m and $\Delta h/h_g = 0.2$, what means a terrain height of 100m above or below the reference plane if it is not at least partially compensated by the tie of the sub-images. This displacement corresponds to only 1.7cm on the ground. The influence in X is even smaller due to the smaller displacement between the two projection centers along the flight direction. In practice, the ratio of $\Delta h/h_g$ only under extreme conditions exceeds the value of 0.2 since this already corresponds to a variation of the object height of 40% in relation the flying height. Normally in such cases separate flight lines will be introduced.

Mean flying height, which is required during DMC post-processing, is normally fixed for one project at the phase of flight planning by the operator. After flight mission it is transferred to the DMC post-processing station. The most common error may be a not correct flying height used during the mosaicking step, which leads to a small

displacement of the single images to the center or to the edge of the virtual image. By combining the images with bundle block adjustment, this effect is compensated by the orientation angles, and therefore a tipping of the single images against the virtual image can be observed. This effect can be compensated by an additional parameter:

$$\begin{aligned} \delta x &= ((0.9 \cdot |x'|) + 1.1 \cdot |y'|) \cdot x' \\ \delta y &= ((0.9 \cdot |x'|) + 1.1 \cdot |y'|) \cdot y' \end{aligned} \qquad (3.2.7\text{-}3)$$

The factors 0.9 and 1.1 are caused by the different extent of the virtual image in column- and row direction. For verification purposes several images with a flying height of 150m (instead of 1500m in the correct case) have been mosaicked. The bundle adjustment with the additional parameter determined this one significantly.

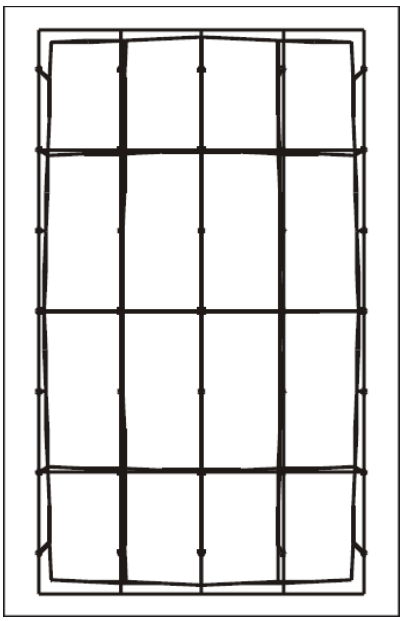

Figure 3.2.6-1: Effect of wrong flying height to the mosaicked virtual image.

3.2.7 Relative Orientation of the Camera Heads

A changing of relative orientation (orientation angles, position of projection centers, focal lengths) of the particular heads during the flight because of vibrations or change of temperature is normally intercepted through bundle adjustment during post-processing, as the relative orientation is computed for every exposure. However a predominating of bad conditions in one exposure concerning for example lightening conditions, poor texture of the surface, repetitive patterns or inappropriate FMC by

theory can influence the quality of tie point extraction and lead to a wrong determination of the relative orientation of one or more images of one particular camera heard during post-processing. This effects to a wrong fusing of the virtual image and can influence the aerotriangulation and adjacent object point determination, if the affected image is used for instance for ground control point measurement. As there is no possibility to model this blunder, it has to be detected during the bundle adjustment at post-processing or during aerotriangulation. Another possibility for verification is plotting all parameters of the relative orientation for the particular heads for the whole block. As normally parameters are very stable over time outliers can be detected easily as wrong determined angles arise as clearly visible peaks.

3.3 Parameter Model

Camera calibration establishes the transformation between object and image space. In most cases a simple projective transformation is not sufficient in terms of accuracy, because of systematic effects. Therefore, additional parameters for building precise mathematic transformation-model (equation 3.3-1) have to be determined. Once the calculated parameters are known, distortion correction can be accomplished [Klaus et al., 2004]. The key to self calibration is to find corresponding points in image sequences of static scenes [Faugeras et al., 1992]. These correspondences are used to determine the internal and external camera parameters simultaneously.

$$
\begin{aligned}
x &= -c\frac{r_{11}(X-X_0)+r_{12}(Y-Y_0)+r_{13}(Z-Z_0)}{r_{31}(X-X_0)+r_{32}(Y-Y_0)+r_{33}(Z-Z_0)} + add\ \ param \\
y &= -c\frac{r_{21}(X-X_0)+r_{22}(Y-Y_0)+r_{23}(Z-Z_0)}{r_{31}(X-X_0)+r_{32}(Y-Y_0)+r_{33}(Z-Z_0)} + add\ \ param
\end{aligned}
\qquad (3.3\text{-}1)
$$

With:

x, y : image coordinates
X_0, Y_0 : projection center coordinates
X, Y, Z: ground coordinates of the object point
r_{ij}: elements of the rotation matrix

Additional parameters have been introduced into the bundle triangulation software package BLUH [Jacobsen, 2007], which are adapted to not only the geometry of the analogue survey camera but also the special geometry of the new digital survey cameras, and used for precise analysis and presentation of the remaining systematic effects.

3.3.1 General additional parameter in BLUH

The Hannover program system for bundle block adjustment BLUH has its own set of additional parameters allowing a compensation of any general type of image deformation. The general additional parameters were developed by Jacobsen [1982], which are difference to the Ebner parameters. The Ebner parameters based on polynomials have disadvantage that the calculated parameters are difficult to analyze, and only optimal if the image points are located in the Gruber points. But Jacobsen parameters describe the physical well-grounded influence directly, and are less correlated like the Ebner set if the image points are randomly distributed.

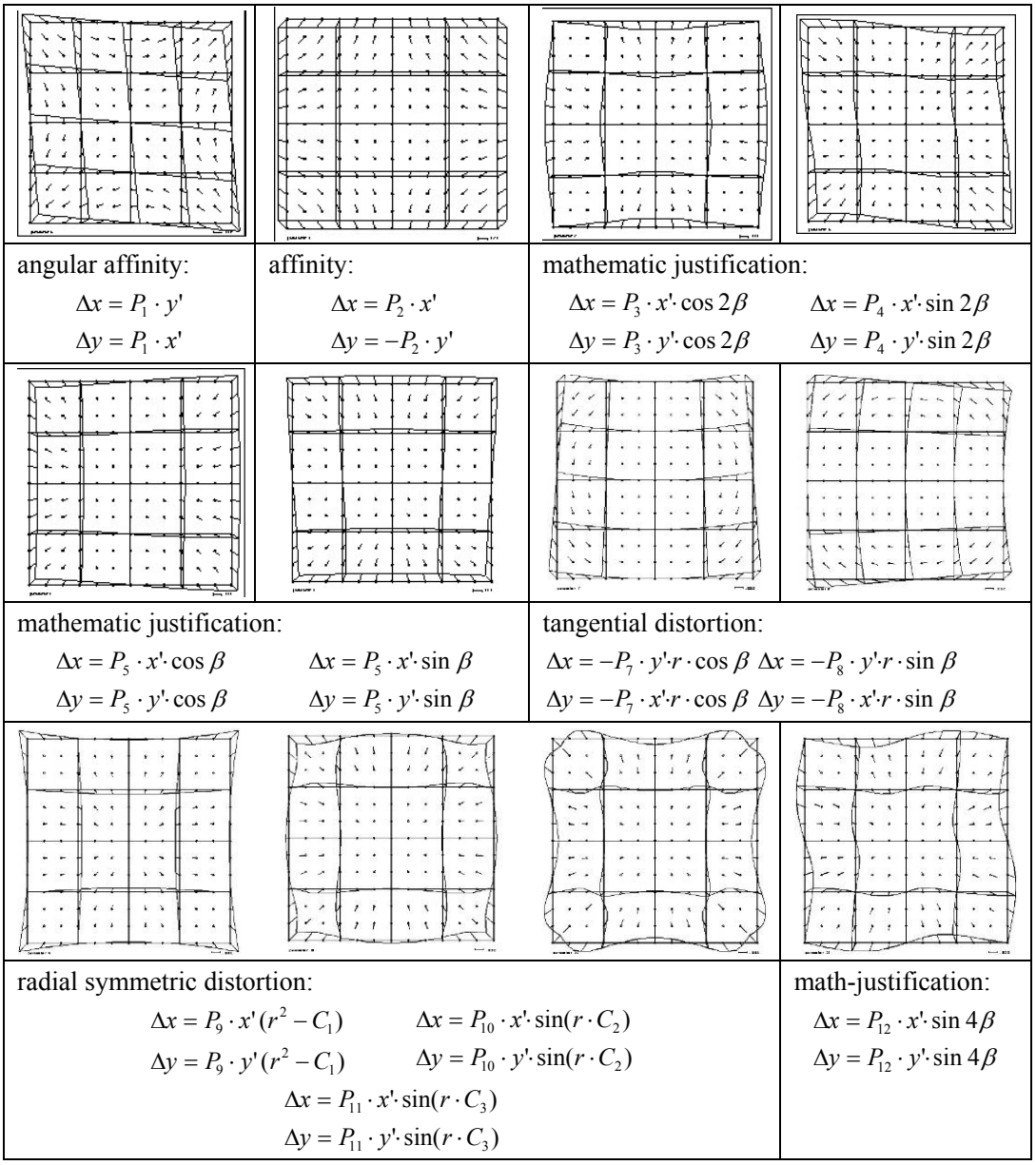

Figure 3.3-1: general additional parameters of program system BLUH

3.3.2 Special additional parameters in BLUH

The new extended parameters have been introduced into the Hannover program system BLUH, which is adapted to the special geometry of the new digital aerial survey cameras. These cameras combine every virtual image from various numbers of sub-cameras and CCD arrays. As for DMC there are two by two sub-cameras. Each sub-camera has its own optical system. Because of convergent view direction a larger field of view is generated by a combination of smaller fields of view. All sub-cameras will be released synchronous. The UltraCam has as well four optical systems for panchromatic exposures. Behind every lens system there are four, two or one CCD

arrays. The four systems are positioned in one line. The instant of exposure is a little time shifted to record every photo at the some position (syntopical). The so-called master-cone has four CCD elements positioned in the corners of the photo. The sensors of the further cameras are positioned to fill all gapes of the master cone. All cameras are mounted parallel for vertical view.

BLUH has a set of Parameters 29-41and 74-80 for modeling the special geometry of the DMC, and a set of parameters 42-73 for UltraCam.

Parameter 29 describes the influence of offset of the 4 panchromatic sub-cameras caused by wrongly defined flying height to the merge of the 4 sub-images (*see figure 3.2.6-1*). It was proved that this parameter was not significant for all handled data sets, showing that no problem with eccentricity errors exist [Jacobsen, 2007a].

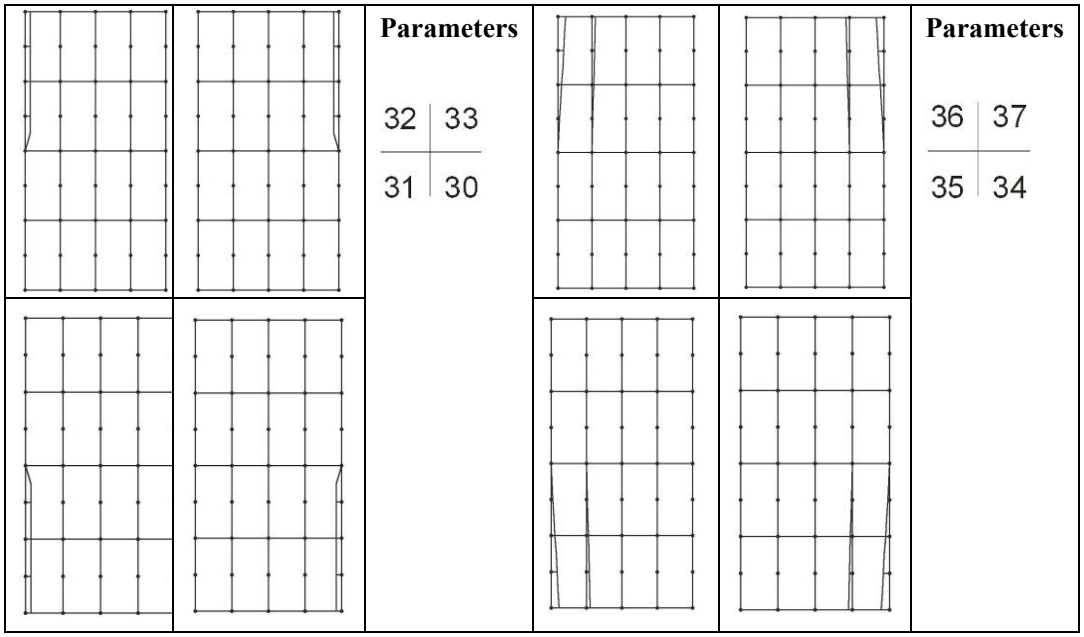

Figure 3.3-2: special parameters 30-37 for DMC

Parameters 30-33 describe the synchronization error of individual cameras. Parameters 34-37 describe x-part of orientation error of individual camera and 38-41 y-part of orientation error of individual camera, i.e. they can determine perspective errors of the sub-images (*see figure 3.3-2 and 3.3-3*). The additional parameters 74–77 can determine radial symmetric effects (r^3) of the DMC sub-cameras (*see figure 3.3-3*). These cameras are rotated against the artificial image plane in the x-direction approximately +/-10.1° and in the y-direction approximately +/-17.9°. The original sub-images do have 4096 x 7168 pixels with a pixel size of 12µm. This relation exists for all the 4 cameras separately and the geometric effect is projected to the artificial image plane. The by far introduced parameters are used to model the geometry of sub-cameras.

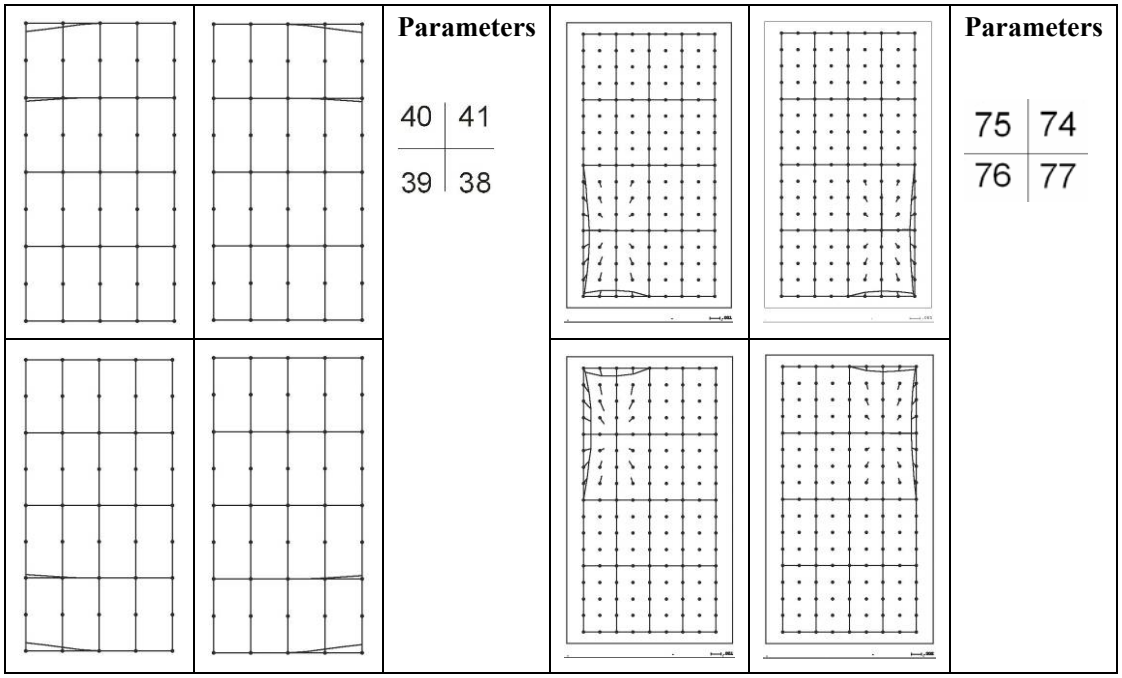

Figure 3.3-3: special parameters 38-41 and 74-77 for DMC

The parameters 78 and 80 describe a common influence of all DMC sub-images (*see figure 3.3-4*). Parameter 78 can compensate the influence of a changed field of view to the virtual images. Parameter 80 determines the r^3 deformation of all sub-images together by just one parameter, respecting the transformation to the plane of the virtual image.

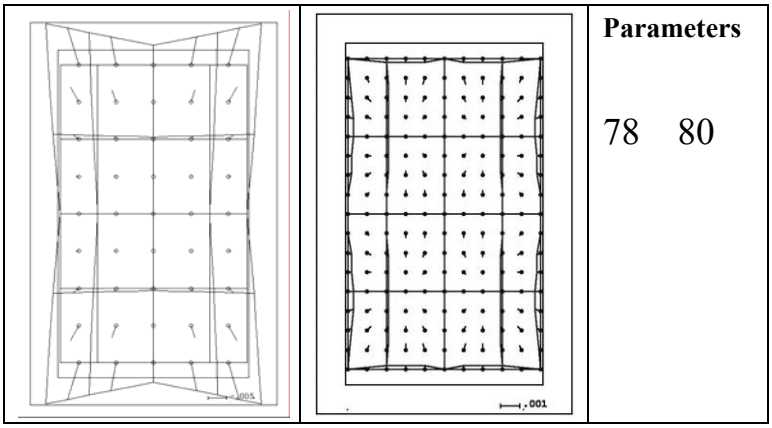

Figure 3.3-4: special parameters 78 and 80 for DMC

Corresponding to the special parameters for the DMC, BLUH includes special additional parameters for handling the geometric problems of the UltraCam. The UltraCam has a virtual image based on 9 individual CCD-arrays. With the additional parameters 42 up to 73 problems of the CCD-array merge can be determined. For 8 different sub-areas special parameters are available. Parameters 42 – 49 are scale parameters for 8 sub-units respectively. Parameters 50-57 and Parameters 58-65 can compensate the influence of shift in x- and y-direction respectively. Parameters 66-73 determine the rotation of 8 sub-units respectively.

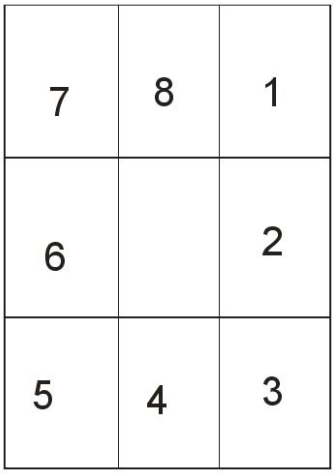

Figure 3.3-5: sub-areas in the image of UltraCam$_D$

The additional parameters are checked by BLUH for individual correlation, total correlation and for significance. Not required parameters are iteratively automatic removed to avoid over-parameterization. [Jacobsen, 1987]

3.4 Outline of Calibration

The influence of systematic image errors is not a new topic for digital images; it exists as well for analogue photos. It's important for the standard digital photogrammetric workflow to know the distortion characteristic of large format digital systems. This task could be performed by means of appropriate test blocks and a self-calibrating or non-self-calibrating bundle block adjustment.

For calibration and analysis of the digital camera systems, the following steps should be done.

- Image collection of a test block in the suited fields.
- Automatic tie point measurement and interactive control point measurement,
- Self-calibrating and non-self-calibrating bundle block adjustment,
- Analysis of the parameters in image and object space
- Analysis of residuals from various observations (image, GPS, GPS/IMU)
- Geometric accuracy assessment and
- Other evaluations (e.g. stability, previous calibrations etc.).

In the proposed geometric test procedure, the system parameters are determined and the geometric accuracy is evaluated. The following quantities characterize the geometric performance of the system:

- The fundamental lens parameters, i.e. principal point (x0, y0) and principal distance(f),
- The geometric distortion characteristics of the camera system; distortions can be modeled using physical, empirical or mixed additional parameters [Förstner et al., 2004],
- The systematic of the image observation residuals before and after self-calibration,
- Misalignments of the sub-systems (camera, GPS, IMU): lever arms and bore sight misalignments,
- The errors in GPS and IMU observations,
- Point determination and back projection accuracy before and after self-calibration.

Well-established physical deformation models are the most attractive option for test field calibration, but in the end the selection of the appropriate model should be based on a detailed analysis of the entire system. Important considerations include the correlation of the parameters and the many physical factors resulting in additional distortions.

Chapter
4. Empirical Analysis

4.1 Introduction

Four data sets were used for the investigation - the blocks Gent, Schwabach, and Rubi were taken with DMC, and Block Istanbul with UltraCamD. The block Gent was computed intensively with different date- and parameter-models and analyzed in detail because the block Gent has a comprehensive configuration with well-proportioned distribution of the control points and precise GPS coordinates of the projection centers.

The analysis has been made in image as well as in object space; the two different ways are introduced in this chapter. The first manner tries to investigate systematic image errors of the camera system *(section 4.3*), the σ_0 – the standard deviation of unit weight – that means the image coordinates and averaged residuals of image observations describe the systematic image errors properly with simultaneous self-calibration with additional parameters. The results of bundle block adjustment without or with self-calibration can indicate the influence on the geometric accuracy in the object space, especially shown at independent check points. The block/model deformation caused also by systematic image errors can have big impact on the generation of digital elevation models (DEM) and the stereo models.

4.2 Data Sets

The parameters of the test blocks play an important role in the block adjustment; they are relevant to the camera system at a certain extent.

Important is the block structure and the ground sample distance (GSD) – the distance of neighbored pixel centers on the ground, determined by the flying height, the focal length and the pixel size in the image. The block structure affects the accuracy and determinability of various parameters. A comprehensive block structure gives the best accuracy and should be used for the most demanding tasks. To be able to determine the principal distance accurately, either the block must contain control points with extensive height differences, or the projection centers must be accurately determined by GPS and located in two different height levels to separate systematic GPS-errors from the influence of the focal length [Jacobsen, 2004]. In the case of analog cameras, the important factor is the imaging scale, because different environmental conditions (pressure, temperature, etc.) at different flying heights affect the system calibration [Jacobsen, 2004]. If well-distributed high accurate control points are available, with the comprehensive block structure the full accuracy potential of digital frame cameras can be tested.

With the mentioned parameters, the selected blocks in the investigation have limitations for analysis of the DMC and UltraCamD geometry. The blocks are introduced in the following section.

Block Gent & Sub-blocks

For the production of true ortho-images, the test block Gent was flown by Hansa Luftbild in summer 2006 (*figure 4.2-1*). The block size of 5.5km × 8.5km includes 1105 images distributed in 27 parallel and 2 transversal strips. Because of the special requirement for the production of true ortho-images, the block has 60% end lap and 80% side lap. The images were taken at a flight altitude of approximately 800m above ground level, the image scale is 1:6540 with pixel size of 12µm corresponding to 7.8cm GSD. Image orientations were directly measured by use of a GPS/IMU system on board of the aircraft. There are 53 full ground control points (GCP) well distributed at the boundary and inside the block. The control points are announced with a standard deviation 3 cm for X, Y and 5 cm for Z. The blocks are stabilized by crossing flight lines allowing a reduction of the number of control points. 23 points (*points with green color*) from GCPs were selected as independent check points.

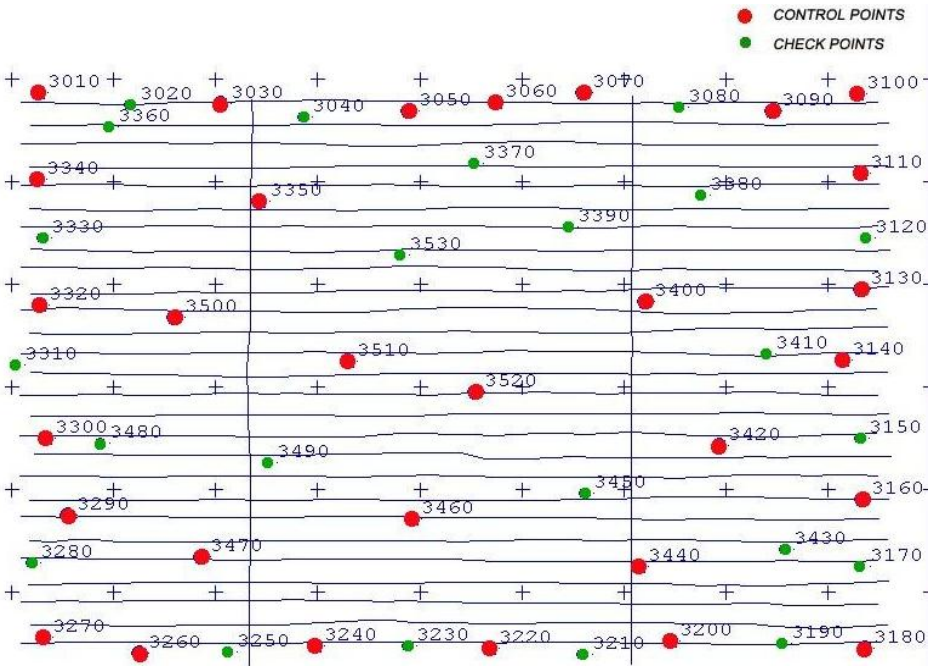

Figure 4.2-1: DMC flight campaign Gent: configuration of flight lines and distribution of control & check points

For the investigation the block Gent with this very high over lap were divided into 3 different sub-blocks, they keep the same size like the original block, and with the same end lap 60% but reduced side lap, respectively 20%, 40%, 60%. The sub-blocks are named Gent_20% with 364 photos, Gent_40% with 442 photos and Gent_60% with 598 photos (*figure 4.2-2*). The reduced sub-blocks are based on the same images, but with different stability of geometry, especially with difference of averaged number of images/points, which could be used to study the interaction between block and digital camera system.

	Gent	Gent_40%	Gent_40%	Gent_20%
images	1105	598	442	364
object points	11899	10677	9916	9285
image points	102132	55706	39877	33113
maximal images/points	21	12	12	9

Table 4.2-1: block configurations

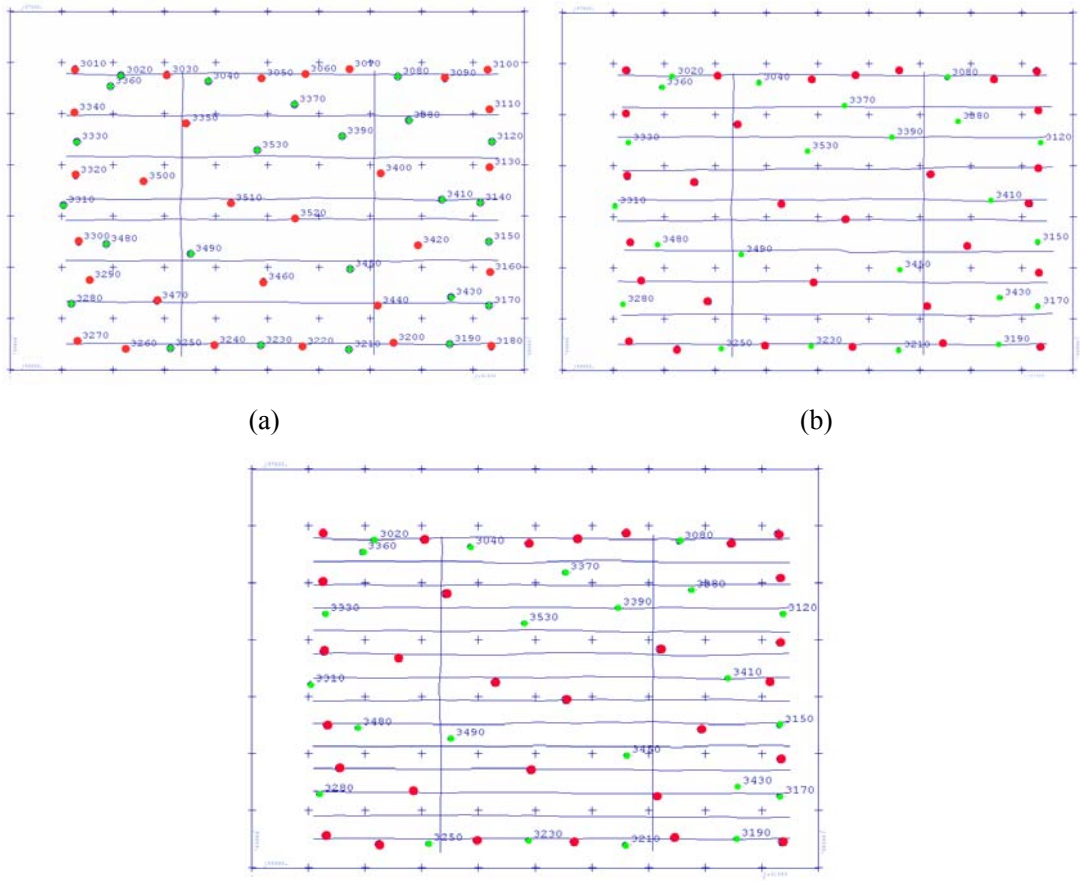

(a) (b)

(c)

Figure 4.2-2: configuration of sub-blocks Gent with different end lap: (a) Gent_20%; (b) Gent_40%; (c) Gent_60%

Block Schwabach

The block Schwabach was flown also by Hansa Luftbild in 2007, the flight mission was taken along southing-northing in a height level of 1382m. Together with the average ground height of 371m the photo scale is 1: 8420, corresponding to 10 cm GSD. The block is shown in figure 4.4-2, and consist 186 photos with 60% side lap and 30% end lap distributed in 9 North-South flight strips. The exterior orientations of photos were directly measured by a GPS/IMU system on the board of aircraft. The GPS coordinates have an announced accuracy 5 cm at all components. 15 full control points and 2 vertical control points were measured with standard deviation of 3cm for horizontal and vertical components. 3 control points were not used for the block adjustment, but as the independent check points to analysis.

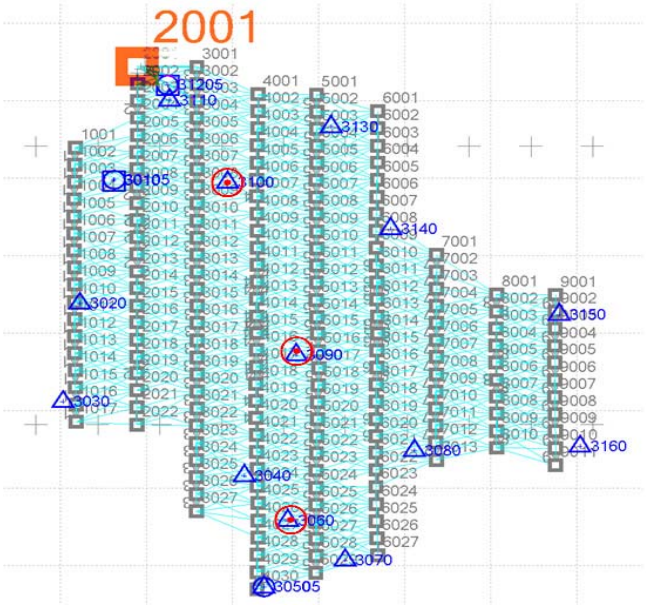

Figure 4.2-2: DMC flight campaign Schwabach: configuration of flight lines and distribution of control and check points

Block Rubi

The block Rubi came from the Institut Cartogràfic de Catalunya (ICC). The images relating to Rubi were acquired on March 8, 2005. The block consists of 426 images having 80% end lap and 40% side lap distributed in 13 parallel and 3 transversal strips (*see figure 4.2-3*). The images were taken at a flight altitude of 1000 m above ground level, the image scale 1:8180 leads with pixel size of 12µm to 10 cm GSD. 426 orientations derived from GPS/IMU data were used to the combined block adjustment. The 39 control points are announced with standard deviation of 2cm for X, Y and 4 cm for Z. 20 of the control points were used as independent check points. The other points with distances up to 12 base lengths were used as control points in the bundle block adjustment. 7763 object and 45464 image points have been matched precisely by use of Intergraph software, corresponding in the average to 5.9 images/point.

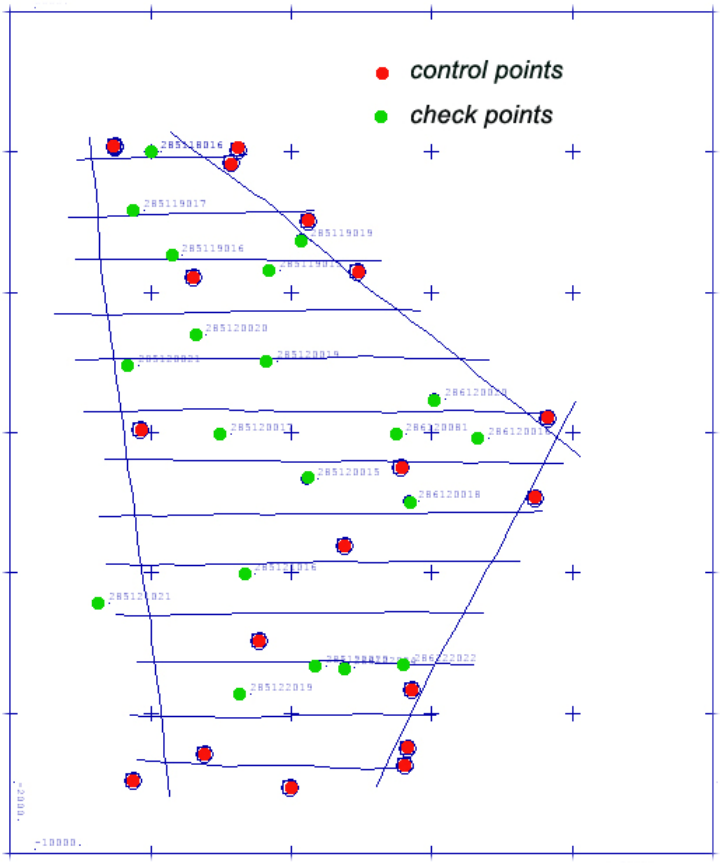

Figure 4.2-3: DMC flight campaign Rubi: configuration of flight lines and distribution of control and check points

Block Istanbul

The city of Istanbul has been flown with the UltraCamD. The block was flown at 3551m height, which together with the average terrain 76m results the photo scale 1:34266. The corresponding GSD is 30.8cm. The block consists of 486 photos; each photo is covering 2.2km x 3.5km. The whole block has a size of 47km x 25km. The configuration of the block is plotted in figure 4.2-4. Control points and check points (respectively with red and green color) were measured with announced 10 cm accuracy. GPS projection centre coordinates are available, having a standard deviation in Z of approximately 50cm.

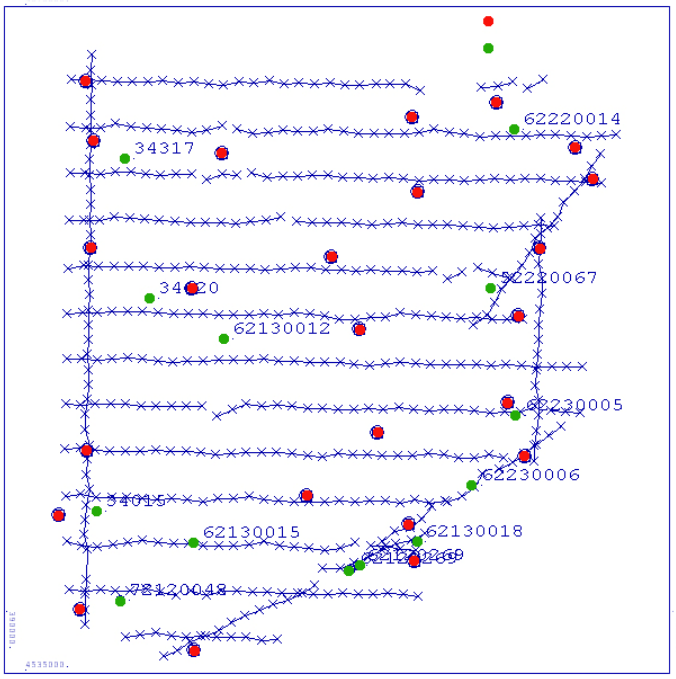

Figure 4.2-4: UltraCam$_D$ flight campaign Istanbul: configuration of flight lines and distribution of control and check points

4.3 Results and Analysis in Image Space

The systematic image errors are influencing the image coordinate residuals of the bundle block adjustment. These residuals are based on systematic and random errors and influenced by the over determination of the block. If all residual are overlaid corresponding to the position of the image points, they are showing the tendency of the systematic errors if the overlaid residuals are averaged in image position sub-areas [Jacobsen, 2007].

Displaying the residuals of the photo measurements of all photos in one single photo frame, systematic effects can be visible. However, this method fails if the number of photo measurements is too high, because nothing can be differentiated anymore because of too many visible vectors. Therefore it makes sense to cover this photo frame with a regular grid and to display just averaged residuals for each grid cell. Of cause this restitution could be done as well mathematically by correlation analysis, but in this case a necessary figure of the geometric corrections isn't available. In the investigation the image was divided into 25×25 cells. The averaged image residuals are analyzed in each grid of the image. The different parameter models were attempted to eliminate the systematic image effects. If the vector distribution of image residuals is random, no systematic image errors or in the case of a block adjustment with self-calibration, no remaining systematic errors exist.

4.3.1 Block Gent

The image measurements of block Gent for aerial triangulation were taken with software MATCH-AT. The 12-bit pixel registration of gray values increased the number of matched tie-points and thus the geometric stability of the block. The image coordinates of control points were measured manually also using Inpho MATCH-AT with an accuracy of approximately 1/3 pixel. 11899 object and 102132 image points have been matched by MATCH-AT; it means that the object points were determined in the average in 8.5 images.

The figure 4.3.1-1-a shows the image measurement of all photos of block Gent overlaid to one single photo frame. The matching processing of MATCH-AT is so designed that the search region of the tie point is be defined in advance. In this manner the matching efficiency can be improved. But it is resulting in a limitation in the investigation that not all parts of the images are used, the systematic image errors in the data gap cannot be determined.

The bundle block adjustments have been made with Hannover program system BLUH. BLUH has its own set of additional parameters which is a combination of parameters

with physical background completed by general parameters to allow a compensation of any general type of image deformation (*section 3.3.1*). The actually used parameters are selected by program based on Student-test and check of correlation [Jacobsen, 1982]. For the exact handling of possible problems caused by the matching of the DMC and UltraCamD sub-images were introduced (*section 3.3.2*).

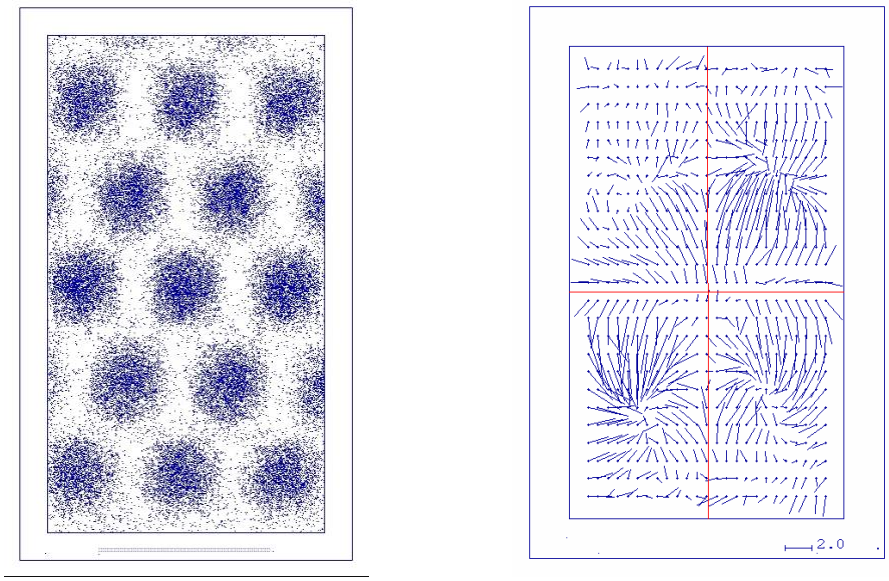

(a) (b)

Figure 4.3.1-1: (a) distribution of image points (overlay of all images), block Gent; (b) averaged image residuals without self-calibration - *vector scale [2µm]*

It may happen that the systematic image errors are changing within the block caused by imaging conditions, by this reason the block Gent has been divided into 2 equal parts and the block adjustment has been made for the whole block, but handling the images as taken by different cameras in BLUH.

The systematic effect is obvious by the results of the bundle block adjustment without self-calibration. The figure 4.3.1-1-b shows the averaged remaining residuals of the sub-images in the virtual DMC image. The image residuals show small rotations clearly in the sub-region and also scale effects. But the high internal accuracy of the block adjustment is indicated by the root mean square discrepancies against the averaged residuals in the image sub-area for RMSx 1.6µm and RMSy 1.5µm corresponding to 0.13 pixels and 0.12 pixels. This is also confirmed by the range of the bundle block adjustment with the standard deviation of unit weight (σ_0) of 2.05µm.

The camera self-calibration with the standard parameters 1-12 can compensate any systematic image errors of usual analogue cameras. They worked well for the multi-sensors DMC-camera. The figure 4.3.1-2-a shows that the systematic effect was

reduced with the set of the general parameters. The σ_0 decreases to 1.75µm from 2.05µm; but still indicating remaining systematic image errors.

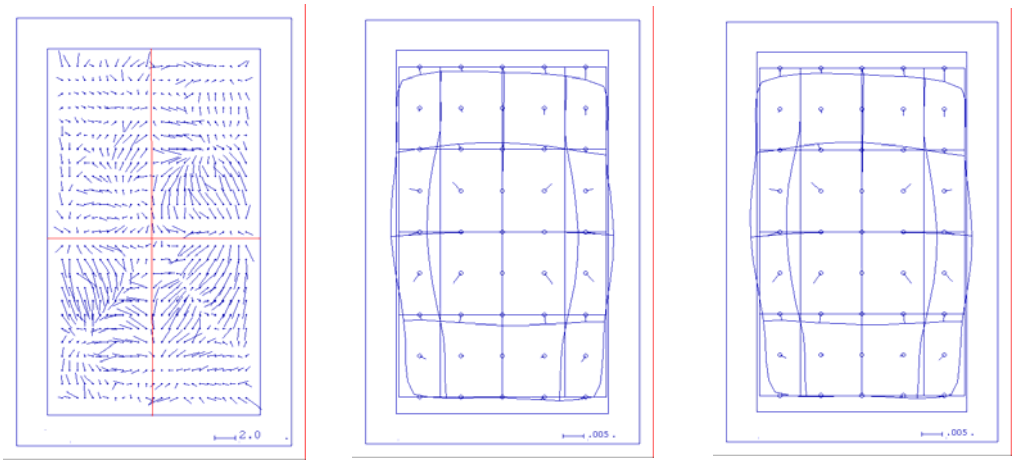

(a) (b) (c)

Figure-4.3.1-2, self calibration using 1-12 parameters: (a) averaged image residuals; (b) systematic image errors of upper sub-block; (c) systematic image errors of lower sub-block

No additional parameters were removed in the block adjustments, almost all parameter are significant in the adjustment. Especially the parameters 9 and 10 modeling the radial symmetrical distortion attract attention; they have Student-test values of 183.6 and 126.9, which indicate the radial symmetrical distortion has very big impact on the systematic image errors of DMC-images. However the radial symmetrical parameters 9 and 10 correlate with the height of projection centers in the combined block adjustment.

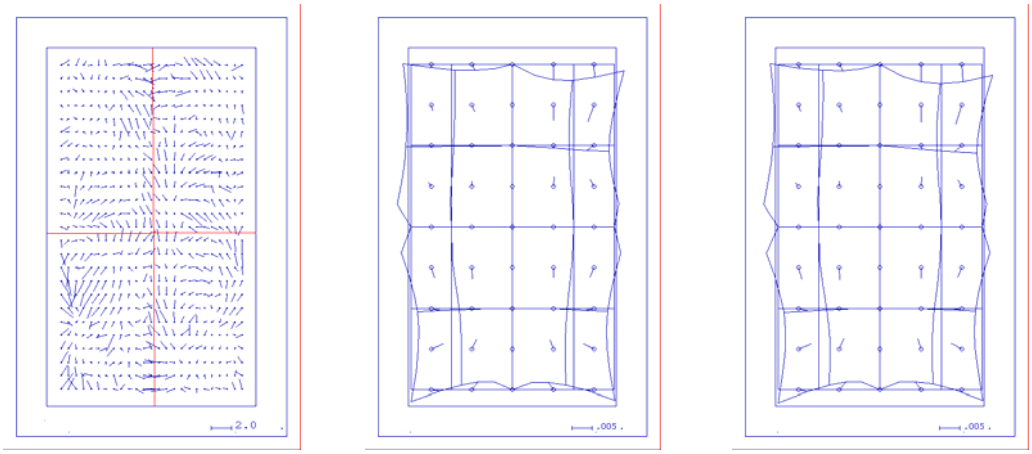

(a) (b) (c)

Figure 4.3.1-3, self calibration using 30-41,74-77 parameters: (a) averaged image residuals; (b) Systematic image errors of upper sub-block; (c) Systematic image errors of lower sub-block

The additional parameters 30-41 and 74-77 are special parameters for DMC cameras. The geometric problem of 4 sub-cameras can be compensated respectively by the set of 16 parameters. The figure 4.3.1-3 shows that the averaged residuals are reduced further with these additional parameters, the σ_0 amounts to 1.63µm. The parameters 74-77 determining radial symmetric effects (r^3) of the DMC sub-cameras have also very big Student-test values of 125.76, 131.16, 71.07 and 141.42; they are much more significant than other additional parameters. Systematic image errors are still remaining in the adjusted image. Because the commonly physical effects available in film cameras like in the DMC, the mathematic model with the standard parameters 1-12 plus parameters 30-41 and 74-77 should be preferred for bundle block adjustment, which was proved by figure 4.3.1-4. The averaged residuals have root mean square values for x and y with only 0.3µm and 0.4µm, which are nearly free from remaining systematic effects. The σ_0 is 1.57µm optimal in all of the bundle block adjustments.

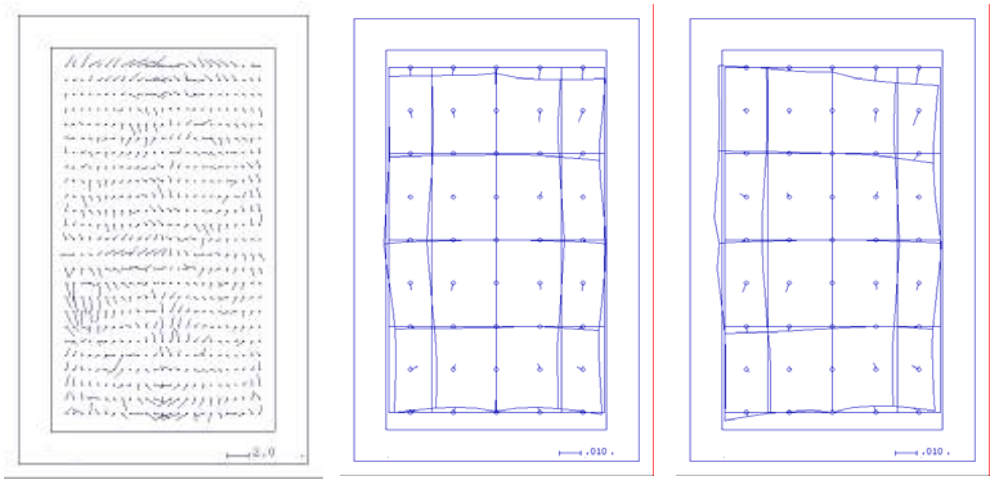

(a) (b) (c)

Figure-4.3.1-4, self calibration using 1-12 + 30-41,74-77 parameters: (a) averaged image residuals; (b) Systematic image errors of upper sub-block; (c) Systematic image errors of lower sub-block

The figure 4.3.1-1-b shows that the averaged image residuals have the similar structure in sub-areas. It is not necessary to use corrections individually for each sub-camera. Under the condition that all 4 sub-cameras are influenced by the same change of the focal length, parameter 78 can compensate the influence of a changed field of view to the virtual image; also with parameter 80 a common change of the radial symmetrical distortion (r^3) of all 4 sub-images with the same size can be respected.

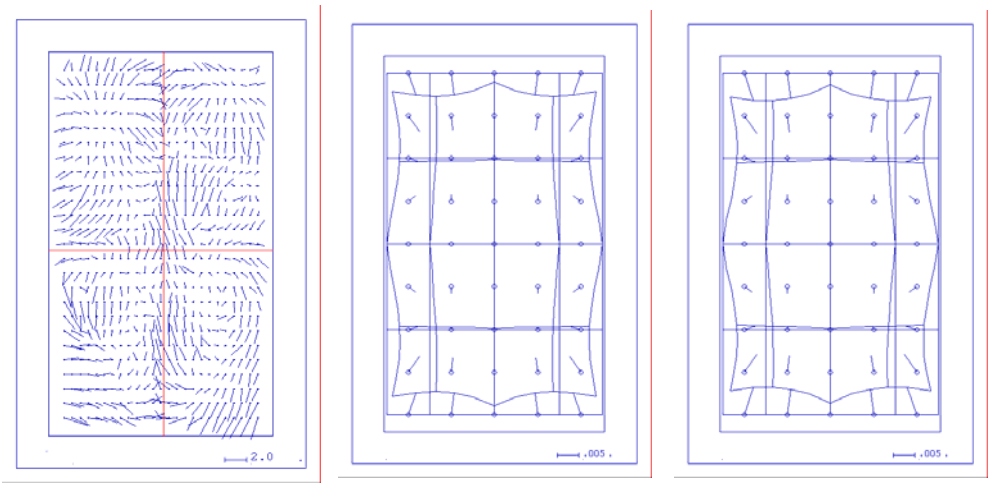

(a) (b) (c)

Figure-4.3.1-5, self calibration using 78, 80 parameters: (a) averaged image residuals; (b) Systematic image errors of upper sub-block; (c) Systematic image errors of lower sub-block

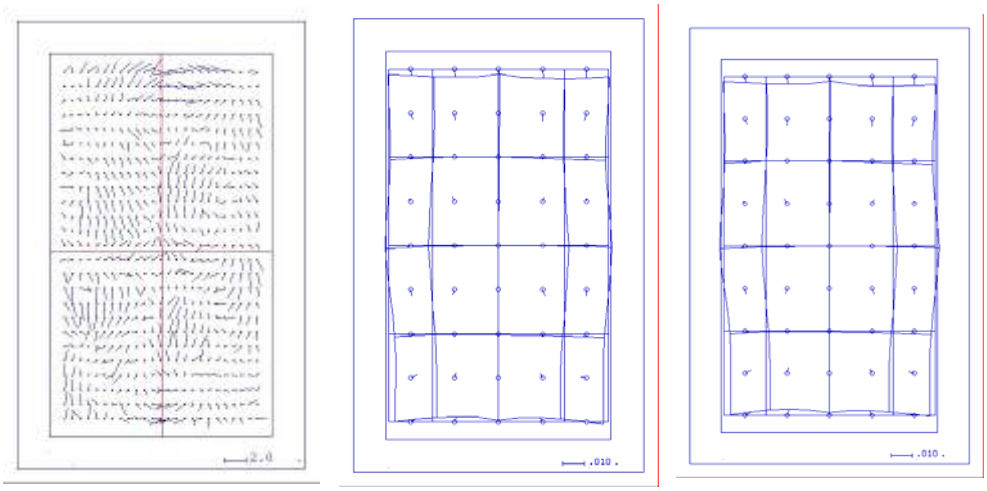

(a) (b) (c)

Figure-4.3.1-6, self calibration using 1-12,78,80 parameters: (a) averaged image residuals; (b) systematic image errors of upper sub-block; (c) systematic image errors of lower sub-block

The figure 4.3.1-5-a shows the averaged residuals are smaller than in the case of the block adjustment without self-calibration. The parameters 78, 80 played big role in adjustment with Student-test values of 66.6 and 199.3. The result was a little worse than with parameters 30-41 and 74-77, because the sub-cameras have some slight difference in systematic effects. The standard parameters 1-12 are still important in this instance; they can reduce the image residuals further together with parameters 78, 80 (*figure 4.3.1-6*).

The plots of image correction show that the systematic image errors of both sub-blocks are nearly identical with root mean square differences of the systematical image errors in the range of 0.5µm up to 1µm. The geometric problems of the cameras are not changing from image to image, and are similar for the whole block of images.

In sub-blocks Gent_60%, Gent_40% und Gent_20%, the number of points per photo are reduced. In Gent_60% the object points are measured in the average in 5.2 images while for the Gent_40% und Gent_20% we have only 4 images/point and 3.6 images/point respectively. The systematic effects of images in the sub-blocks should be same because they are based on the same images, but the figure 4.3.1-7 displays that the blocks with higher overlap and much more tie-points show the systematic image errors more obviously. It shows that larger parts of the systematic errors in smaller sub-blocks can be compensated by the exterior orientation and the over determination of the object points. But the general trend of the systematic image errors agrees.

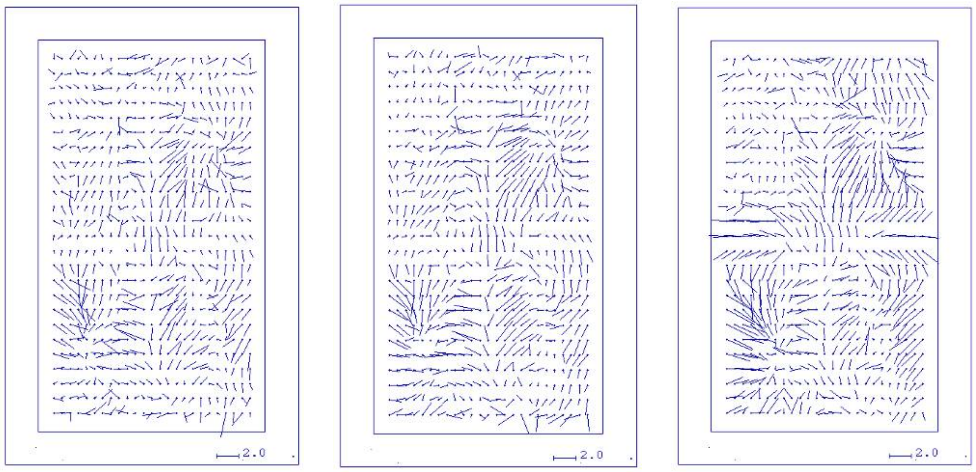

(a) (b) (c)

Figure-4.3.1-7, averaged image residuals of sub-blocks without self calibration: a)Gent_20%; b) Gent_40%; c) Gent_60%

4.3.2 Other DMC-Blocks

The block Schwabach is typical for the mapping. The image measurement was also taken with MATCH-AT. 6612 object points and 22180 image points were matched precisely.

The image points of block Schwabach are distributed in the Gruber areas. Because of less redundancy and the matching mode, there are even the data gaps in the image sub-areas (*figure 4.3.2-1*). The σ_0 for the block adjustment without self- calibration is only 1.35µm, and the plot of the averaged image residuals shows only small systematic effects. It is proved again that in small blocks large parts of the systematic errors can be compensated by the exterior orientation and the smaller over determination of the object point.

Block Rubi is a better instance, the image points were matched well-proportioned in all image area. The figure 4.3.2-2 shows similar systematic effects in the image but a little smaller like the Gent block. After the same manner of block adjustments, the results of block Rubi are similar to the block Gent. The accuracy of the image coordinates is in the same range and also the tendency of the dependency upon the additional parameters agrees.

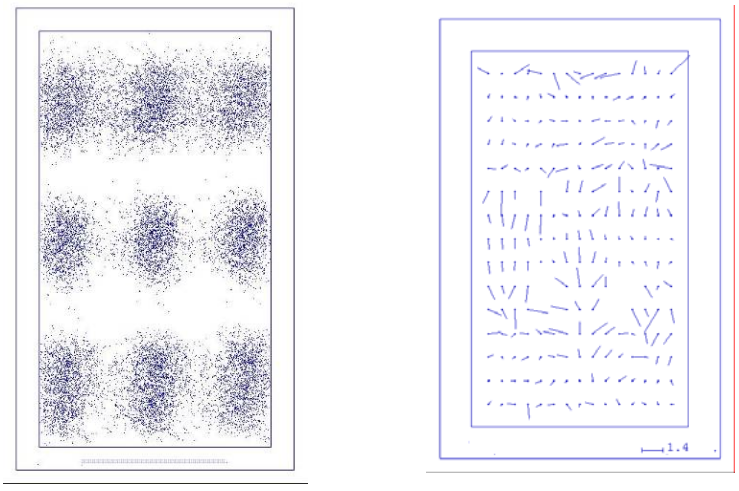

(a) (b)

Figure-4.3.2-1, block Schwabach: (a) distribution of image points (overlay of all Images); (b) averaged image residuals without self-calibration - *vector scale [1.4µm]*

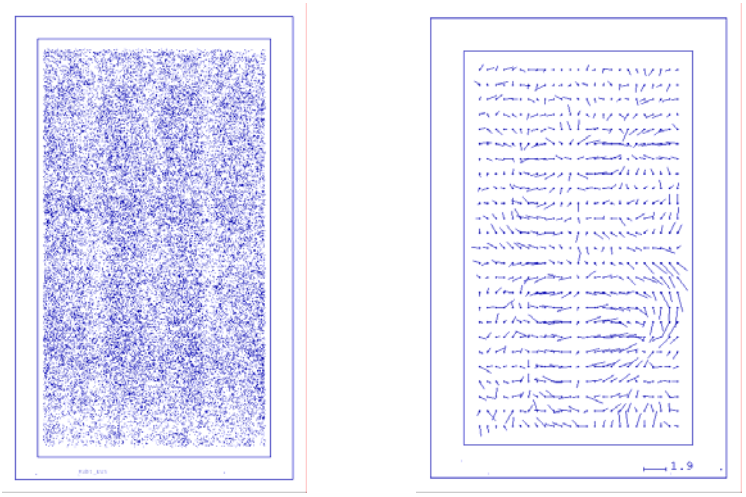

(a) (b)

Figure-4.3.2-2, block Rubi: (a) distribution of image points (overlay of all Images); (b) averaged image residuals without self-calibration - *vector scale [1.9µm]*

4.3.3 Block Istanbul

Block Istanbul is the only UltraCamD-block in this investigation. The block adjustment has been handled in the tangential system to avoid problems with the earth curvature and map projection. The 1843 object points and 8556 image points are corresponding to 4.6images/point. The averaged residuals are plotted in figure 4.3.3-1, indicating the shape of remaining systematic image errors. With the general additional parameters, the size of the averaged residuals is reduced, but the shape remains. Even here remaining systematic image errors still exist after block adjustment with the general additional parameters 1-12 together with the special parameters 42-73 for UltraCam System.

(a) (b) (c)

Figure-4.3.3-1, block Istanbul - averaged image residual of block adjustments - *vector scale [3µm]*: (a) without self-calibration; (b) with parameters 1-12; (c) with parameters 1-12, 42-73.

After stitching panchromatic sub-images to the virtual image, if the calibration of the master image is correct, the systematic errors should be limited to effects caused by the optics. The scale variations, shifts and rotations of the sub-images are causing different effects in the virtual image of UltraCam. If the geometric problems are only based on the merge of correct sub-images, the systematic image errors could be handled just with the special parameters for UltraCam, with the parameters 42 up to 73 fitting the 8 sub-images to the centre image (*section 3.3.2*).

The systematic image errors of UltraCamD were illustrated in the figure 4.3.3-2. The bundle block adjustments with self-calibration by additional parameters with standard set of additional parameters leads to systematic image errors. The radial symmetric parameter 9 dominates with T-test values of 15.56. The other large T-values are shown for affinity effects parameters 1 and 2 with values 6.41 and 10.94. In the case of self calibration with the standard BLUH-parameters together with the special UltraCam-parameters 42-73, the radial symmetric distortion is also the dominating systematic effect, but parameters 1 and 2 were removed in the adjustments based on student-test and check of correlation, instead of them the special UltraCam-parameters were preferred by BLUH.

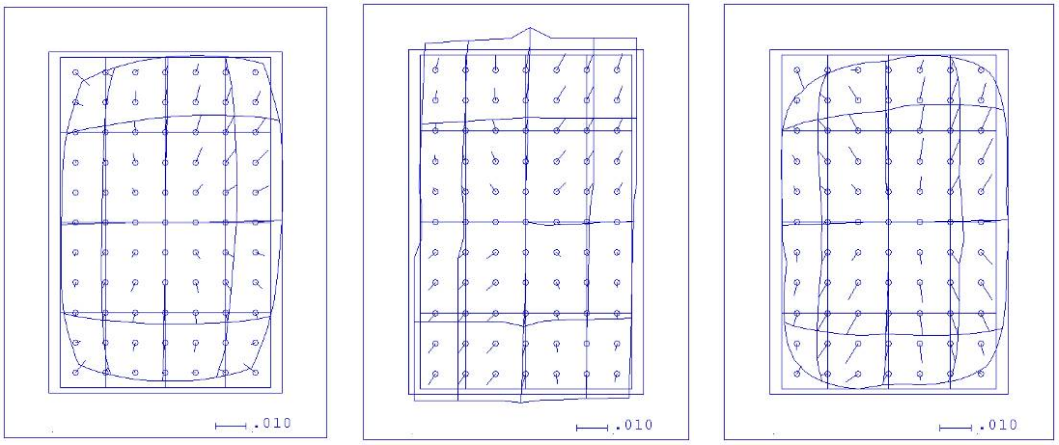

(a) (b) (c)

Figure-4.3.3-2, block Istanbul - systematic image errors: (a) with parameters 1-12; (b) with parameters 42-73; (c) with parameters 1-12, 42-73.

It should be mentioned that the systematic image errors of the UltraCamD are stable – at least within the block. The figure 4.3.3-3 shows that a handing of two sets of images together in one block adjustment was leading to negligible differences of the systematic image errors between both sub-blocks [Jacobsen, 2007].

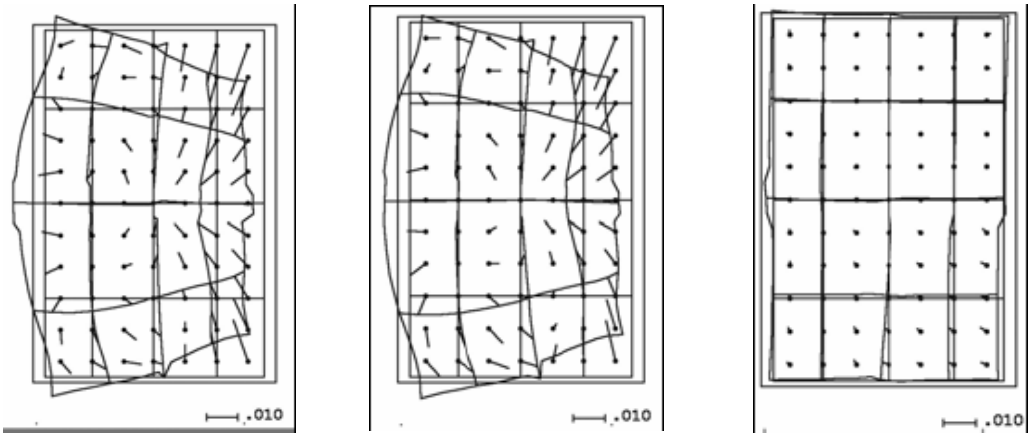

(a) (b) (c)

Figure 4.3.3-3: UltraCamD-block "DSK-Saar": systematic image errors of flight campaign day1 (a) and day2 (b), difference of systematic image errors day1-day2 (c). [Spreckels et al., 2007]

4.3.4 Conclusion

The high accuracy potential of digital aerial frame cameras has been confirmed with standard deviations of unit weight σ_0 in the rage of approximately 2µm for the Intergraph DMC and approximately 3.5µm for the Microsoft Photogrammetry UltraCamD, corresponding respectively to 0.15 GSD and 0.4 GSD. This is quite better like with analogue photos. Not negligible systematic image errors are present in the DMC-images as well as in the UltraCamD-images. The bundle block adjustment with the basic set of the BLUH-parameters can eliminate the largest amount of the systematic image errors, but for a complete determination the special DMC -parameters and UltraCam-parameters are required in addition. The averaged residuals for the UltraCamD are approximately 3 times larger than for the DMC and a more detailed fine structure exists – caused by the combination of 9 sub-images to one virtual image, and in addition also the combination of all additional parameters does not totally eliminate the systematic effects for UltraCamD-camera. In the case of the DMC the systematic errors common for all 4 sub-cameras together cover the largest part of the systematic errors; this is an important fact for an improved camera calibration which may reduce the systematic effects in advance.

The averaged residuals from a bundle block adjustment without self-calibration are clearer in the case of a block with higher overlap. Large parts of the systematic errors can be compensated by the exterior orientation and the lower over determination of the object point in the case of smaller end and side lap.

4.4 Results and Analysis in Object Space

By bundle block adjustments with additional parameters, the systematic effects could be determined and respected almost in all blocks. The averaged image residuals show only the effect in image space. The inner accuracy of the block adjustment usually is too optimistic and does not respect systematic errors. The more important question is the influence of the systematic image errors to the accuracy of the ground coordinates, whether the additional parameters play a significant role to improve the accuracy of ground coordinates in the block adjustment. The check points are able to evaluate the accuracy of the bundle block adjustment.

4.4.1 Block Gent

23 points of the original control points were selected as independent check points in the block Gent and not used as control points. The distance of the control points is in the range of 4 – 10 base length related to 60% end lap (*see figure 4.2-1*). The bundle block adjustments with different conditions for block Gent were inspected with BLUH. The results are listed in table 4.4.1-1.

	σ_0 [µm]	Control points [cm]			Check points [cm]		
		RMSX	**RMSY**	**RMSZ**	**RMSX**	**RMSY**	**RMSZ**
without GPS-Data							
without self-calibration	2.05	2.6	3.1	15.3	2.4	2.9	19.1
with parameter 1-12	1.73	2.2	3.1	3.8	2.7	2.2	5.9
with 30-41, 74-77	1.63	2.4	3.1	4.2	2.2	3.2	6.6
with 1-12 and 30-41, 74-77	1.57	2.2	3.1	3.1	2.6	2.2	5.7
with 78, 80	1.73	2.5	3.0	5.5	2.5	2.9	7.5
with 1-12 and 78, 80	1.62	2.2	3.1	3.8	2.6	2.3	6.1
with GPS-Data (with additional parameters 13-18)							
without self-calibration	2.23	2.9	3.3	4.6	2.6	3.2	6.0
with 1-12	1.84	2.6	3.2	5.0	2.6	2.1	6.0
with 30-41,74-77	1.75	2.7	3.4	4.5	2.2	3.4	5.5
with 1-12 and 30-41,74-77	1.68	2.6	3.1	4.8	2.5	2.1	5.6
with 78, 80	1.85	2.9	3.1	5.2	2.5	2.8	6.4
with 1-12 and 78, 80	1.73	2.6	3.2	5.1	2.6	2.1	6.0
a priori Standard deviation: σ_0 = 2.0µm for image points; S_{XY} = 3.0cm, S_Z= 5.0cm for control points; S_{XY} = 5.0cm, S_Z= 5.0cm for GPS project centers.							

Table 4.4.1-1: results of bundle block adjustments block Gent with 60% end lap and 80% side lap

The results show the discrepancies at the control point based on the adjusted orientation and a common intersection – this is a realistic estimation of the problems at the control points not splitting of the error component of the image coordinates. Most programs are showing only an unrealistic small part of the discrepancies which can be manipulated very easy to any result. By this reason a comparison of the results cannot be based on the root mean square discrepancies at the control points, only a comparison with independent check points is realistic.

In the case of the block adjustments without support of GPS projection centers, the horizontal accuracy is not so much influenced by the self-calibration. The root mean square difference (RMS) in all cases amounts to approximately 0.3 GSD for the horizontal components. But without self-calibration the big discrepancy was shown in the Z of independent check points, the RMSZ is 19.1cm corresponding to 2.4 GSD. A block adjustment with self-calibration is obviously required. The RMSZ is in the range of 5.7cm up to 7.5cm, corresponding to 0.7 up to 1 GSD. It is interesting that the same accuracy at the independent check points has been reached with the combination of the general parameters with just the 2 additional parameters 78 and 80 like with the individual DMC-parameters. That means that the DMC systematic errors common for all 4 sub-images modeled by 78, 80 can cover the largest part of the systematic errors.

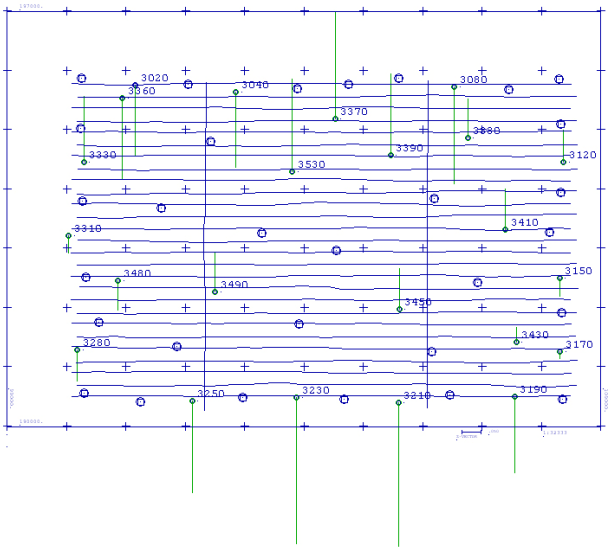

Figure 4.4.1-1: Z-discrepancies at check points of block adjustment without self-calibration, block Gent

The Z-discrepancies of individual check points are much larger close to the block periphery than inside the block (*see figure 4.4.1-1*). By block adjustments with additional parameters or in the case of combined adjustments with GPS-data, the Z-discrepancies are reduced obviously, shown in figure 4.4.1-2.

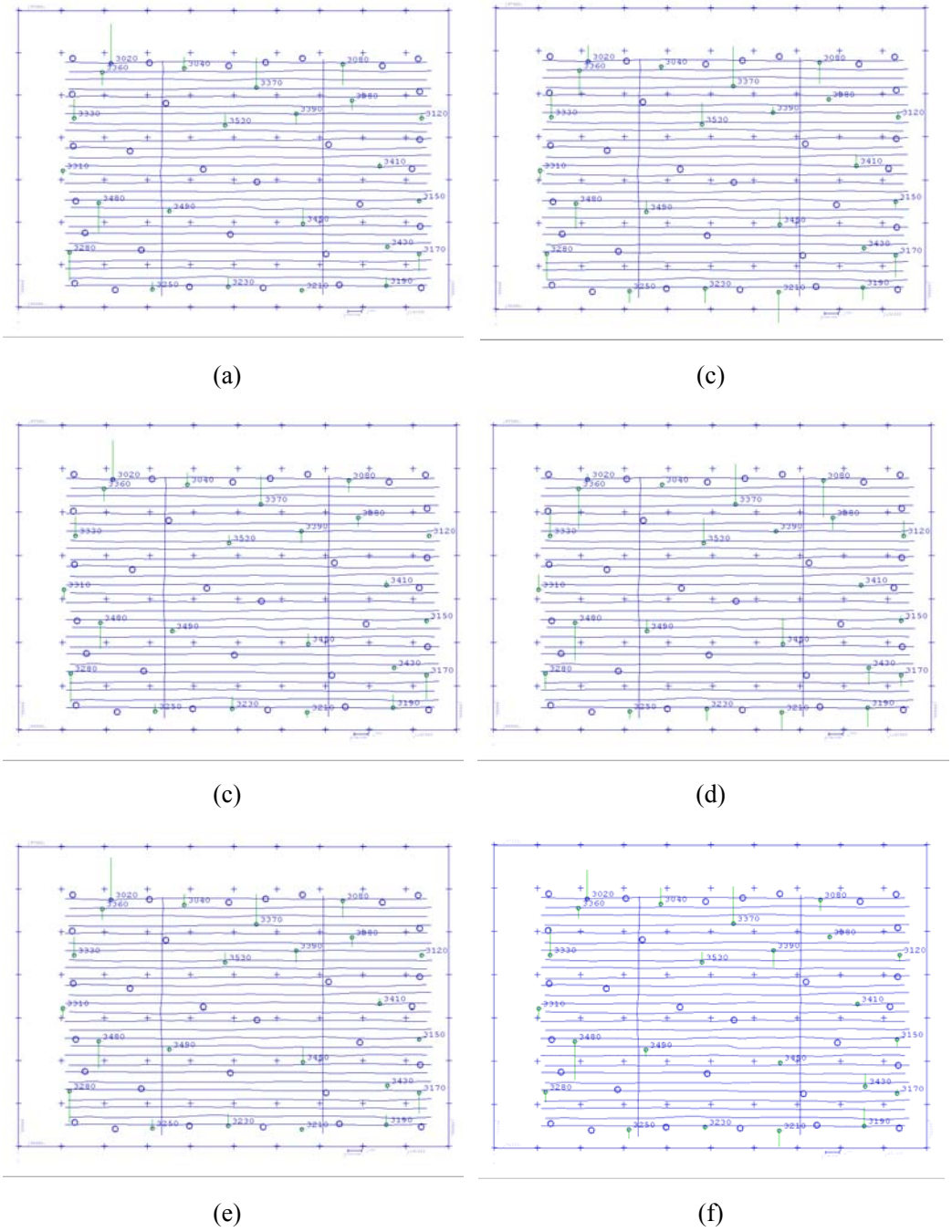

(a) (c)

(c) (d)

(e) (f)

Figure 4.4.1-2, Z-discrepancies at check points of block adjustment block Gent: (a) with parameters 1-12; (b) with parameters 30-41, 74-77; (c) with parameters 1-12 and 30-41, 74-77; (d) with parameters 78, 80; (e) with parameters 1-12 and 78,80; (f) with GPS-data, no self-calibration.

We pay more attention to the combined block adjustment with precise differential GPS-data. All observation types must refer to the same map projection. In most cases, GPS still have some shift and drift effects - systematic offsets of GPS. Reason for necessary drift corrections are an unknown GPS antenna eccentricity or the ground station not being in the project area during the photo flight. Another reason might be

the not correct ambiguity solution for kinematic GPS-survey. Those offsets can be determined with the additional parameters 13-18 of program BLUH. Parameters 13-15 compensate the GPS-shift in Z-, X- and Y-direction, and 16-18 compensate the GPS-drift in Z-, X- and Y-direction. The drift correction requires a suitable amount of ground control points or crossing flight lines for reliable computation. The correction should not be used; if not enough control points or crossing flight lines are available. The shift and drift correction in the program BLUH is computed strip wise. Two sets of correction coefficients are computed: linear corrections and constant corrections (*see figure 4.4.1-3*).

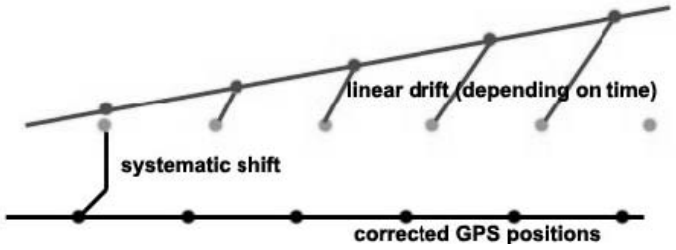

Figure 4.4.1-3: GPS offsets

The results of combined block adjustments with precise differential GPS-data for the whole block Gent are listed in table 4.4.1-1 and also in figure 4.4.1-4. The good result was obtained in the combined block adjustments without self-calibration. The additional parameters could only slightly improve the point accuracy. The RMSX and RMSY amount to 0.3 GSD in the all sets and the RMSZ always to the range of 0.8 GSD. The systematic image errors are relevant with the exterior parameters; therefore they can not always be declarative. It means that the block deformation caused by systematic image errors is mainly compensated by the GPS projection centers.

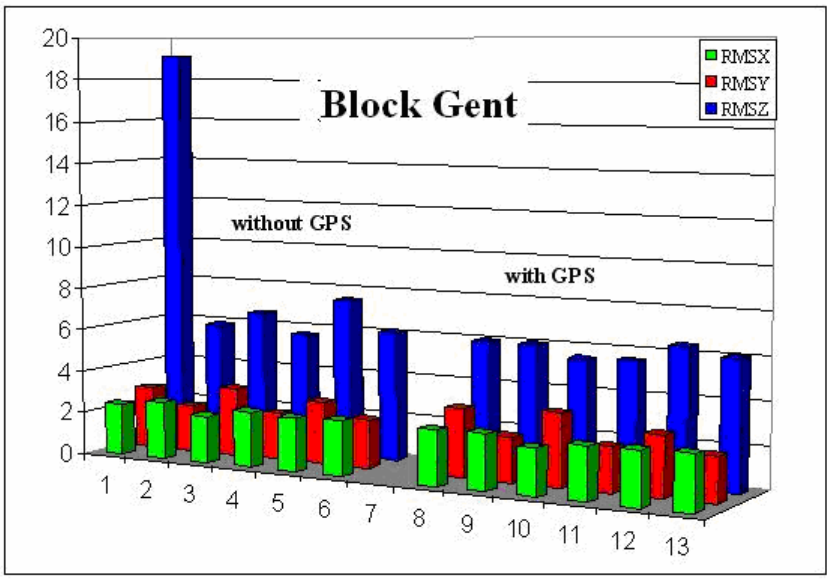

Figure 4.4.1-4: root mean square differences at check points

In image space large parts of the systematic errors can be compensated by the exterior orientation and the over determination of the object point in the blocks with less overlap. But in the object space the geometry of the blocks with high overlap und more tie-points are more stable, so a better accuracy of object points can be obtained. This is proved by means of the combined block adjustments of the sub-blocks Gent based on the same images.

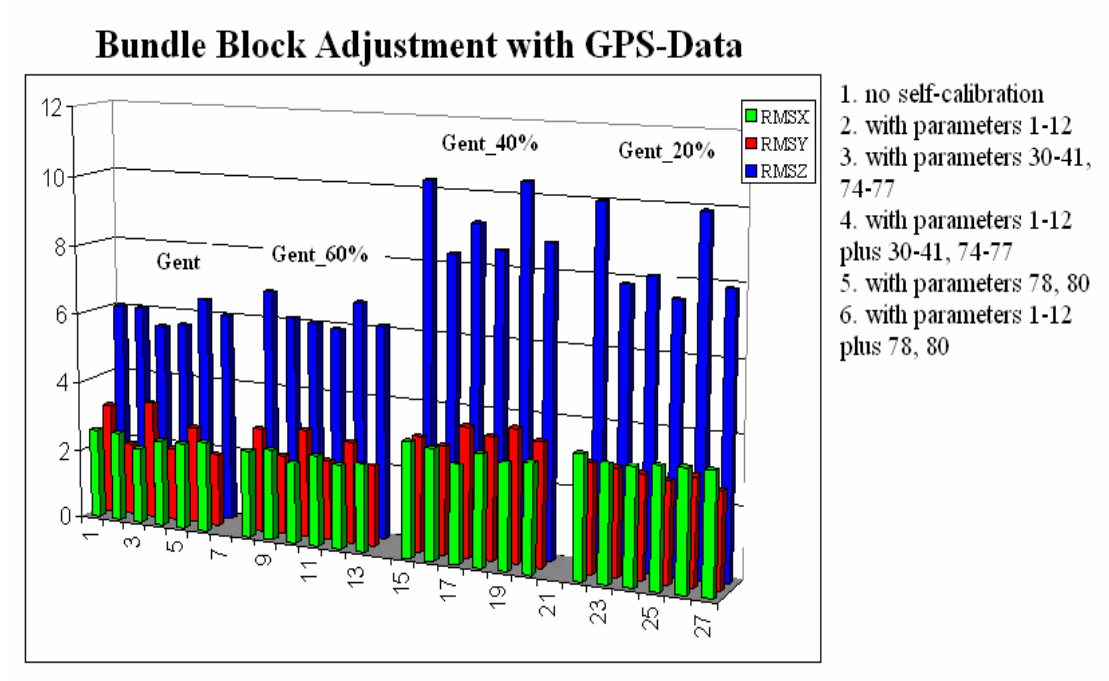

Figure 4.4.1-5: root mean square differences at check points at the combined block adjustments for block Gent

The figure 4.4.1-5 shows that by bundle block adjustments with the same set of additional parameters for the blocks based on the same image with higher overlap and higher redundancy, the better accuracy can be achieved at the independent check points. It means that not only the precise GPS project centers can reduced the effect of the systematic image errors to the ground position, but also the higher number of images per point and high overlap. The main effect to ground coordinates is not only the systematic image error itself.

The high number of images per point of course is improving the result – for the horizontal location this should be depending upon the square root of the number of points – explaining the difference in accuracy between both block configurations.

4.4.2 Block Schwabach & Block Rubi

The results of the block Schwabach are listed in table 4.4.2-1, which shows the self-calibration is necessary in the adjustments without GPS as well as in the combined adjustments. But in the adjustments without GPS the systematic image errors lead to large high deformation, with GPS-data this effect can be reduced.

	σ_0	Check points [cm]		
	[µm]	**RMSX**	**RMSY**	**RMSZ**
without GPS-data				
without self-calibration	1.21	2.0	3.3	18.1
with parameters 1-12	1.18	1.4	3.1	8.9
with GPS-data				
without self-calibration	1.35	1.4	3.1	10.4
with parameters 1-12	1.33	1.4	2.7	6.3

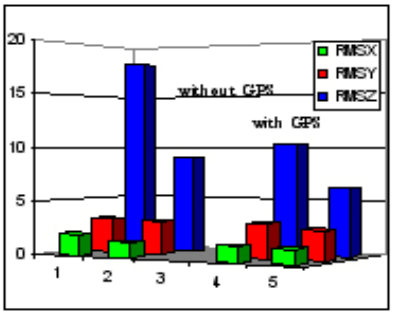

a priori standard deviation: σ_0 = 2.0µm for image points, S_{XY} = 3.0 cm, S_Z= 3.0 cm for control points, S_{XY} = 5.0 cm, S_Z= 5.0 cm for GPS

Table 4.4.2-1: results of bundle block adjustments block Schwabach

The block adjustment of Rubi has been handled in the tangential system to avoid problems with the earth curvature and map projection. The results are listed in table 4.4.2-2. The block Rubi has a high overlap with 80% end lap, 40 side lap, comparable to the block Gent.

	σ_0	Check points [cm]		
	[µm]	**RMSX**	**RMSY**	**RMSZ**
without GPS-data				
without self-calibration	1.90	3.1	2.7	8.7
with parameters 1-12	1.82	2.3	2.6	6.2
with parameters 1-12,30-41,74-77	1.75	2.5	2.8	4.9
with parameters 1-12 78, 80	1.76	2.4	2.9	4.9
with GPS				
without self-calibration	2.04	3.2	2.9	5.5
with parameters 1-12	1.93	3.1	2.9	6.1
with parameters 1-12,30-41,74-77	1.86	3.5	3.4	6.5
with parameters 1-12 78, 80	1.88	3.3	3.3	6.0

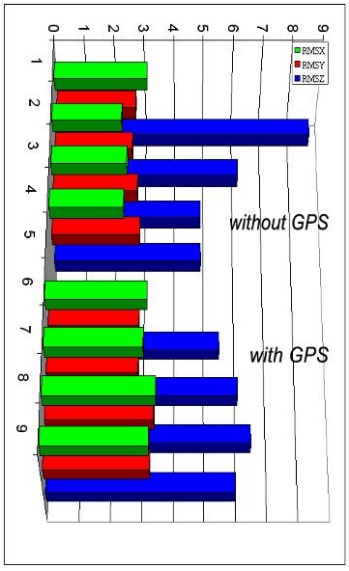

Standard deviation: σ_0 = 2.0µm for matching image points, σ_0 = 4.0µm for manual image points , SXY = 2.5 cm, SZ= 4.0 cm for control points SXY = 10.0 cm, SZ= 10.0 cm for GPS

Table 4.4.2-2: results of bundle block adjustments block Rubi

The blocks Rubi and Gent have a stable geometry, the general additional parameters as well as the special DMC parameters play no role in the combined block adjustments of the block Rubi, because the systematic image errors are relatively small, its main effects act on the vertical component, which can be compensated very well supported by GPS-data. The systematic image errors have a larger influence on blocks with smaller overlap, the block adjustments should be supported by the additional parameters that can eliminate the main effects.

The Blocks Schwabach and Rubi have the same GSD of 10cm; in both blocks 0.3 GSD in planimetry and 0.6 GSD in altimetry for the object coordinates can be achieved.

4.4.3 Some Results with MATCH-AT

The block adjustments of block Gent based the same object observations and image observations like shown before have been made also with MATCH-AT, where Ebner parameters [Ebner, 1976] and Grün parameters [Grün, 1978] can be used in the bundle block adjustments.

The Ebner parameters are a set of 12 correction terms. The 12 correction terms are orthogonal to each other in order to keep the dependence of their parameters among each other and towards parameters of the exterior orientation as low as possible. They are able to compensate systematic errors that are appearing in 9 image points (3 x 3 distributed in the image plane – Gruber points). The 44 parameters of Grün can be seen as an expansion of the Ebner parameter set, as they can model a systematic error that is appearing at a grid 5 x 5 image points.

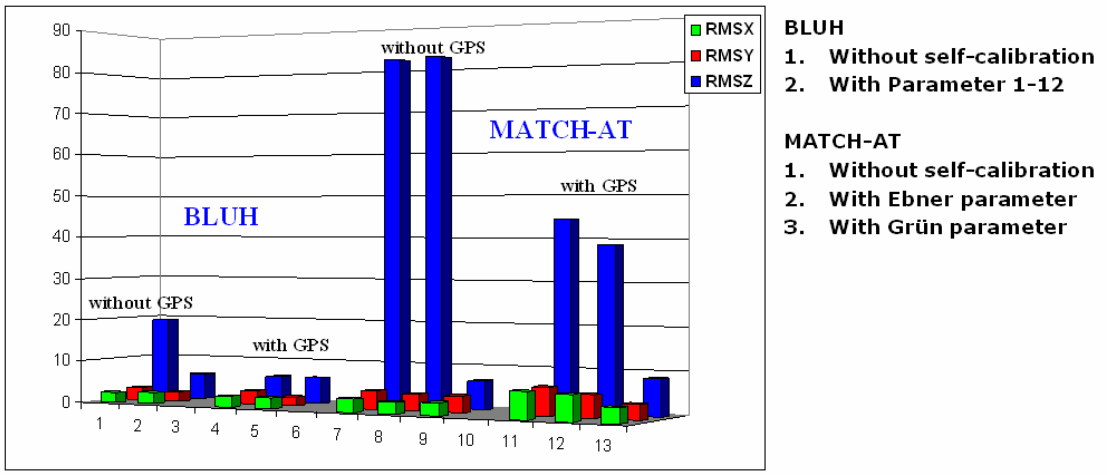

Figure 4.4.3-1: comparison of the block adjustments for block Gent with BLUH und MATCH-AT

	σ_0	Check points [cm]		
	[µm]	**RMSX**	**RMSY**	**RMSZ**
without GPS, no add. param.	1.7	3.1	4.3	82.2
without GPS, Ebner param.	1.7	2.8	4.0	82.6
without GPS, Grün param.	1.5	3.0	3.9	6.7
with only GPS	1.9	6.4	6.6	44.5
with GPS and Ebner param.	1.8	6.1	5.4	38.6
with GPS and Grün param.	1.5	3.6	3.6	8.6

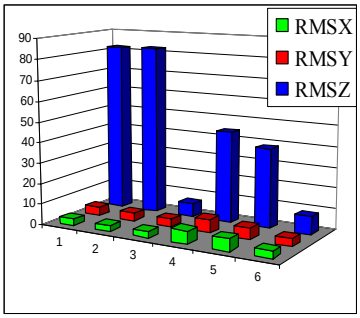

a priori standard deviation: σ_0 = 2.0µm for matching image points, σ_0 = 4.0µm for manual image points , SXY = 3.0 cm, SZ= 5.0 cm for control points SXY = 5.0 cm, SZ= 5.0 cm for GPS

Table 4.4.3-1: results of bundle block adjustments block Gent with MATCH-AT

The results of block adjustments are listed in table 4.4.3-1. Although based on the same observations, the block adjustments without self-calibration by MATCH-AT and BLUH obtained very different results for the independent check points – the RMSZ achieved at independent check points is quite higher for MATCH-AT like for BLUH. The systematic image errors in MATCH-AT indicate exceptional effects on the vertical component, without support by GPS; the RMSZ reached even 10 GSD in the block adjustments without self-calibration and with Ebner parameters in comparison to 2 respectively 1 GSD reached with BLUH. Only with the Grün parameters the systematic effects can be eliminated well, the obtained accuracy is 0.3 GSD in X, Y and 0.8 GSD in Z, the same range as achieved with BLUH. The reason may be that the Ebner parameters with 3 x 3 image points are not able to detect the systematic effects, but with dense 5 x 5 image points (Grün parameters) the systematic effects can be covered and eliminated.

The block Schwabach has been made also with MATCH-AT; the results show some difference with BLUH.

	σ_0	Check points [cm]		
	[µm]	**RMSX**	**RMSY**	**RMSZ**
without GPS				
without self-calibration	1.2	1.7	4.6	23.3
with Grün parameters	1.1	1.8	3.0	6.5
with GPS				
without self-calibration	1.2	4.6	4.9	2.6
with Ebner parameters	1.1	4.1	4.5	2.3
with Grün parameters	1.1	3.9	4.1	2.8

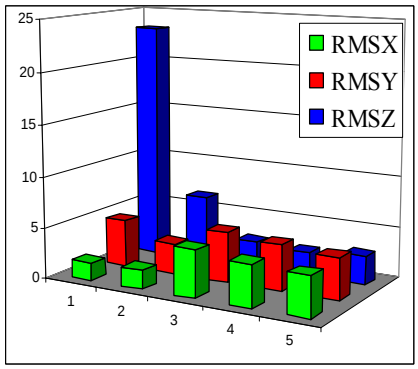

a priori standard deviation: σ_0 = 2.0µm for matching image points, σ_0 = 4.0µm for manual image points , SXY = 3.0 cm, SZ= 5.0 cm for control points SXY = 5.0 cm, SZ= 5.0 cm for GPS

Table 4.4.3-2: results of bundle block adjustments block Schwabach with MATCH-AT

4.4.4 UltraCam-Block Istanbul

The block adjustments for block Istanbul have been handled in the geographic coordinate system and tangential system. The results are listed in the table 4.4.4-1. Because of a small photo scale the influence of the earth curvature and map projection to object accuracy is possible to exist. The adjustment handled in tangential coordinate system and pre-correction by refraction correction can avoid the problems. Such a strict orthogonal coordinate system corresponds to the mathematical model.

	σ_0 [µm]	Control points [cm]			Check points [cm]		
		RMSX	**RMSY**	**RMSZ**	**RMSX**	**RMSY**	**RMSZ**
in geographic coordinate system							
without self-calibration	3.80	9.4	9.8	15.2	23.8	39.5	157.5
with parameters 1-12	3.61	6.9	8.2	8.4	16.4	28.0	91.5
with parameter 9	3.67	9.0	8.6	9.8	21.2	35.3	100.9
with parameters 9 plus 42-73	3.56	6.9	7.3	7.9	15.8	27.7	84.1
with parameters 1-12,42-73	3.56	7.1	7.2	7.9	16.7	27.4	86.0
in tangential coordinate system							
without self-calibration	3.88	9.7	10.5	16.6	24.7	41.5	179.4
with parameters 1-12	3.60	6.9	8.4	8.0	16.4	27.8	93.8
with parameter 9	3.67	9.0	8.8	9.4	21.8	26.2	102.1
with parameters 9, 42-73	3.56	6.9	7.4	7.9	15.2	26.9	85.0
with parameters1-12, 42-73	3.56	7.0	7.4	7.9	16.8	27.4	88.2

Table 4.4.4-1: results of bundle block adjustments block Istanbul

The results show that the earth curvature and map projection have only limited influence on the block adjustments.

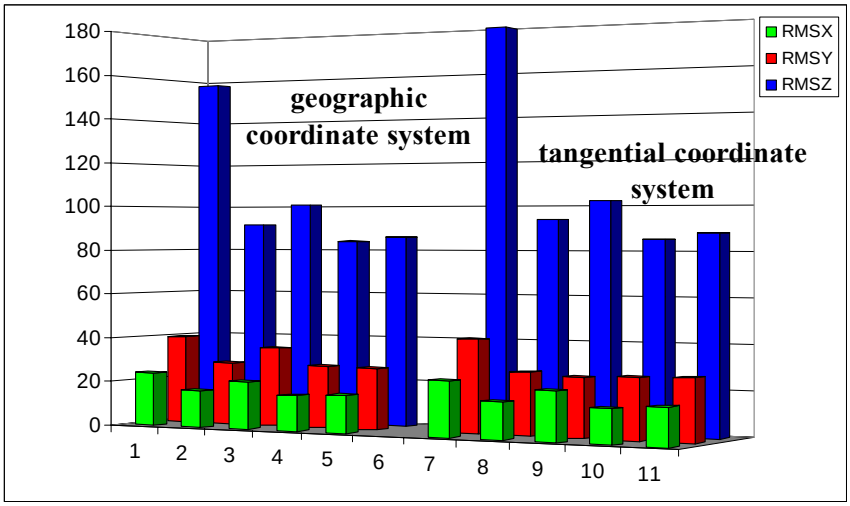

Figure 4.4.3-1: results of bundle block adjustments block Istanbul

The control point distribution of block Istanbul is below the limit which usually can be accepted. The control point configuration with 24 control points has to bridge up to 20 base lengths. The sparse control is sensitive for systematic image errors which can sum up and cause especially a height deformation of the block. By this reason the sparse control is useful for the investigation of remaining systematic effects.

The requirement of self-calibration by additional parameters is obvious even for the handling in a tangential coordinate system and pre-correction by refraction correction. As shown in table 4.4.4-1, there is no clear advantage of the special UltraCam-parameters 42-73 against the standard 12 additional parameters of the program BLUH. With only parameter 9 or combined together with the special UltraCam-parameters 42-73 the same range of accuracy have been reached like with the standard BLUH parameters 1-12. The radial symmetric distortion by r^3 (additional parameter 9) is very important, by this reason this parameter has been used in any case and with a student test value of approximately 32.2 there is no doubt for the requirement.

The ground sample distance (GSD) is 31cm, the height to base relation 3.76. With sufficient control point density and distribution the vertical accuracy should be 3.76 times the horizontal accuracy if the points are located in a stereo model; but the object points are located in 2 up to 10 images, in the average in 4.6 images. By this reason the vertical accuracy is better than the announced accuracy. The sigma0 in image space is in the range of 0.4 pixels. In object space the horizontal accuracy at independent check points corresponds up to 0.7 GSD, vertical accuracy 2.7 GSD, indicating results was limited by the accuracy and distribution of the available control points.

4.5 Block/Model Deformation

The large frame digital camera systems have a high accuracy potential, but systematic image errors exist in the DMC-images as well as in the UltraCamD-images. Systematic image errors are causing block deformation as well as model deformation. The main effect is in the vertical component, but also the horizontal changes have to be checked. For most precise ground coordinates the bundle block adjustment is used, while for mapping the horizontal accuracy is usually not a problem. This may be different for the height, especially for digital elevation models (DEM) generated by automatic image matching or manual stereo plotting.

4.5.1 Comparison of Block Adjustments of DMC-Blocks

The block Gent was used intensively to investigate the block and model deformation caused by systematic image errors. The quality of block adjustment is mainly depending upon the tie points, connecting the image. Gaps in the connection can cause local geometric problems. The block Gent has a large overlap, and the tie points are measured averagely in 8 images. Figure 4.4.5-1 shows with the color coded number of images per point the good image connection. The geometry of block Gent is very stable.

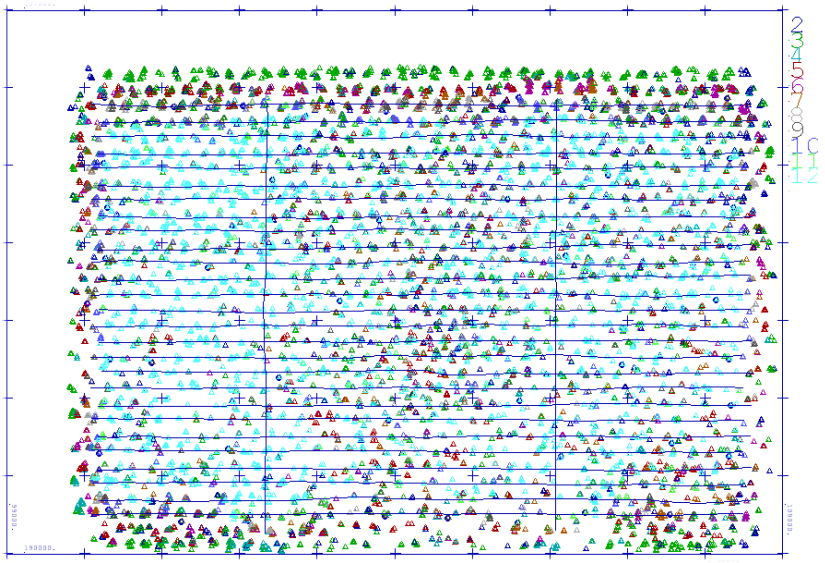

Figure 4.4.5-1: distribution of object points in the whole block Gent, color coded number of images per point.

Because of the large distance of control points the block deformation caused by systematic image errors is obviously through comparison of object points based on the bundle block adjustments. The figures 4.4.5-2 (a), (b) and figures 4.4.5-3 (a), (b), (d),

(e) show that the bundle block adjustments with GPS-data or with set of additional parameters are able to eliminate main part of block deformation. The effect to horizontal coordinate components is very small, the squares mean difference of all object points for all comparison is only approximately 1.5cm; it brings no problem for mapping tasks.

.

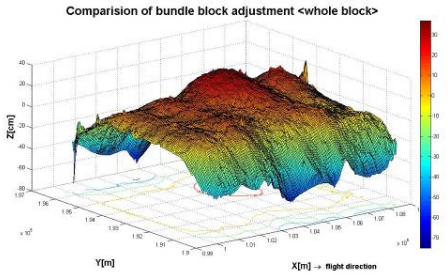

(a) RMSX=1.2, RMSY=2.7, RMSZ=19.5 cm

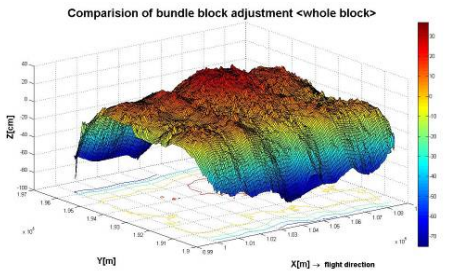

(b) RMSX=1.0, RMSY=1.3, RMSZ=23.5 cm

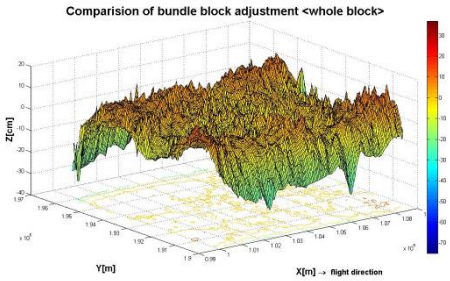

(c) RMSX=1.4, RMSY=2.3, RMSZ=6.6 cm

Figure 4.4.5-2, comparison of bundle block adjustments –whole block Gent: (a) without GPS-data, no self-calibration against with GPS-data, no self-calibration; (b) without GPS-data: no self-calibration against parameters 1-12; (c) with GPS, no self-calibration against without GPS, parameters 1-12. ***[scale range: -75cm up to 35cm]***

The block adjustment without self-calibration shows an obvious high deformation, it is a large problem for the generation of DEMs. The reason is that the systematic image errors make an impact on the block not strongly supported by control points, which leads to a bending of block. The combined block adjustments supported by GPS-data are able to avoid the summation of systematic effects in the no-control-points zone, and so the high deformation can be inhibited. The general additional parameters and special DMC-parameters of BLUH are also able to eliminate the main part of the systematic errors in each image to avoid the high deformation. This was proved through the comparison of different sets of block adjustments for block Gent (*figures 4.4.5-3*). The DMC-block Rubi is comparable with block Gent, because they have the same range of GSD and high accuracy of the available control points. The comparison of bundle block adjustments shows a very similar tendency as block Gent (*figures 4.4.5-4*).

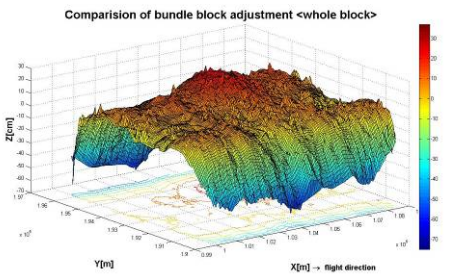

(a) <RMSX=0.7, RMSY=1.2, RMSZ=18.1; (cm)>

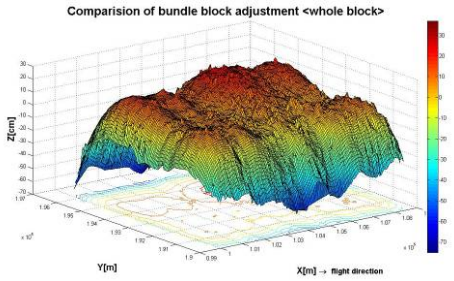

(b) <RMSX=0.6, RMSY=0.9, RMSZ=18.4; (cm)>

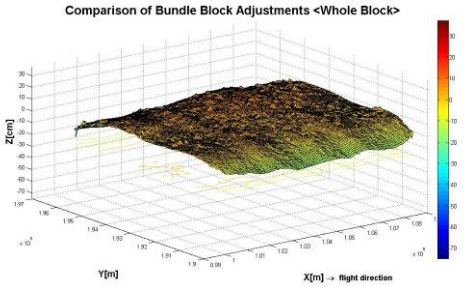

(c) <RMSX=0.6, RMSY=1.7, RMSZ=5.4; (cm)>

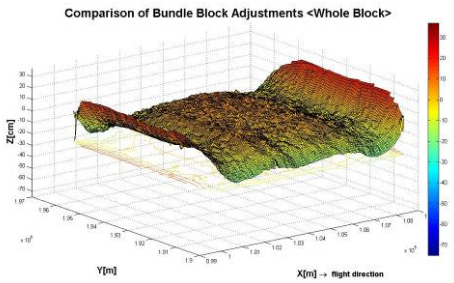

(d) <RMSX=0.7, RMSY=1.4, RMSZ=7.0; (cm)>

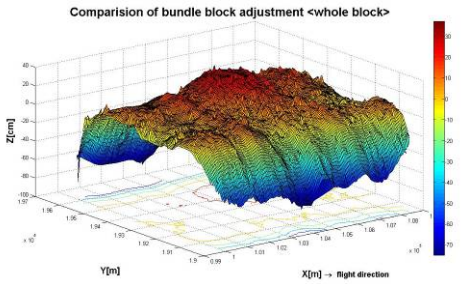

(e) <RMSX=1.0, RMSY=1.4, RMSZ=23.6>

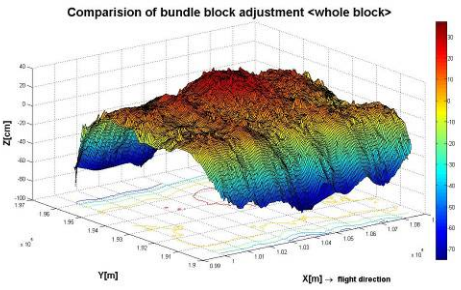

(f) <RMSX=1.0, RMSY=1.5, RMSZ=23.3>

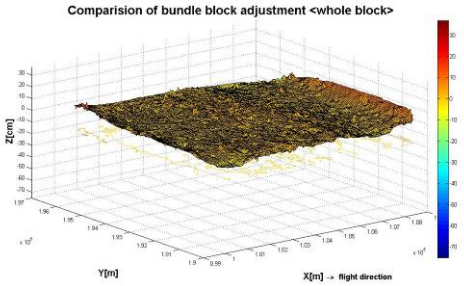

(g) <RMSX=0.4, RMSY=0.5, RMSZ=2.0; (cm)>

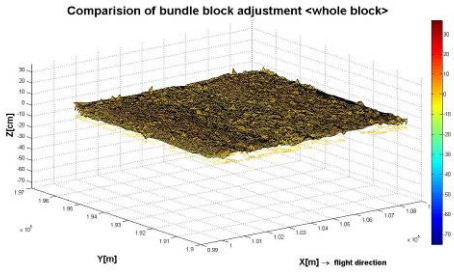

(h) <RMSX=0.3, RMSY=0.5, RMSZ=1.0; (cm)>

Figure 4.4.5-3, comparison of bundle block adjustments without GPS-data against whole block Gent: (a) no self-calibration – parameters 30-41, 74-77; (b) no self-calibration – parameters 78, 80; (c) parameters 30-41,74-77 – parameters 1-12 and 30-41,74-77; (d) parameters 78,80 – parameters 1-12 and 78,80; (e) no self-calibration – parameters 1-12 and 30-41, 74-77; (f) no self-calibration – parameters 1-12 and 78, 80; (g) parameters 1-12 – parameters 1-12 and 30-41, 74-77; (h) parameters 1-12 – parameters 1-12 and 78, 80. ***[scale range: -75cm up to 35cm]***

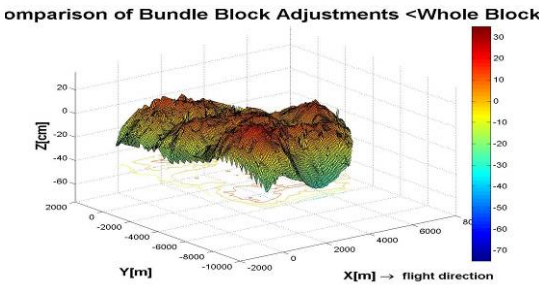

(a) <SX=1.5, SY=1.3, SZ=8.8; (cm)>

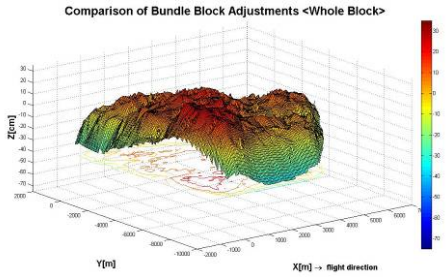

(b) <SX=1.7, SY=2.1, SZ=12.3; (cm)>

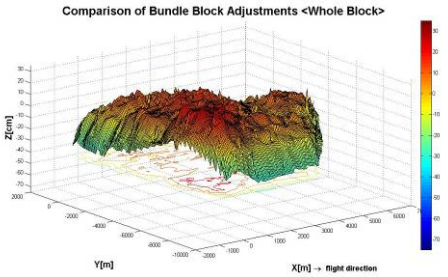

(c) <SX=1.6, SY=2.5, SZ=11.7; (cm)>

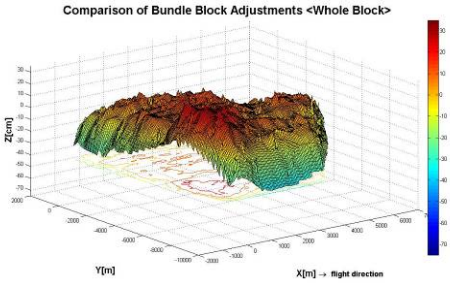

(d) <SX=1.7, SY=2.0, SZ=11.9; (cm)>

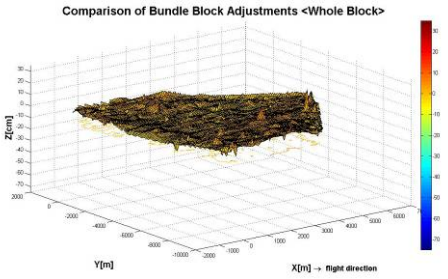

(e) <SX=0.6, SY=1.0, SZ=1.8; (cm)>

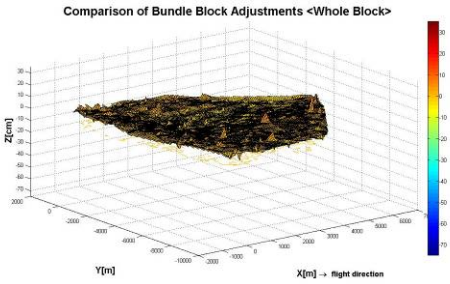

(f) <SX=0.6, SY=0.9, SZ=1.7; (cm)>

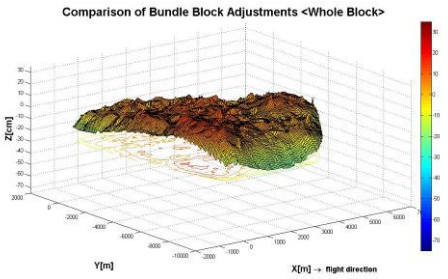

(g) <SX=1.8, SY=1.4, SZ=7.3; (cm)>

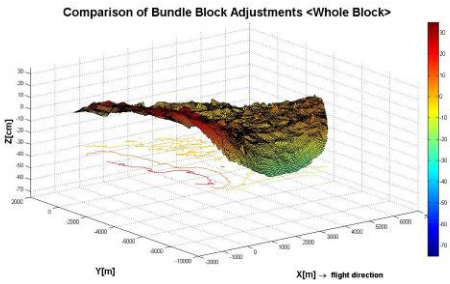

(h) <SX=1.7, SY=1.9, SZ=8.4; (cm)>

Figure 4.4.5-4, comparison of bundle block adjustments without GPS-data against whole block Rubi: (a) without GPS-data, no self-calibration – with GPS-data, no self-calibration; (b) no self-calibration – parameters 1-12; (c) no self-calibration – parameter 1-12 and 30-41, 74-77; (d) no self-calibration – parameters 1-12 and 78, 80; (e) parameters 1-12 – parameters 1-12 and 30-41, 74-77; (f) parameters 1-12 – parameters 1-12 and78, 80; (g) parameters 30-41, 74-77 –parameters 1-12 and 30-41, 74-77; (h) parameters 78,80 – parameters 1-12 and78, 80. ***[scale range: -75cm up to 35cm]***

By combined block adjustment the model deformation usually caused by the systematic image errors is avoided by the exterior orientation, so the systematic effects are reduced or eliminated by the combined block adjustments. In block adjustments with self-calibration the additional parameters are also correlated with each others. It is interesting in these cases that the adjustments based on different mathematical models eliminate the deformation in similar extent. The special DMC-parameters 30-41 & 74-77 as well as 78, 80 have only a limited influence to the object coordinates, because the results based on the standard parameters 1-12 and the results based on the standard parameters plus special DMC-parameters are not too different. This indicates that the geometry of the DMC is stable, and not so much influenced by systematic image errors. The special geometry of multi-sensors and mosaiking processing results in only very limited systematic effects. The main effect is caused by a block deformation and not a deformation of the model itself.

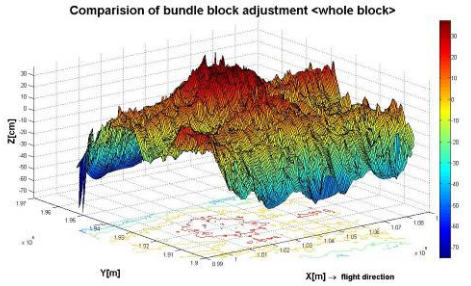

(a) RMSX=1.8, RMSY=1.9, RMSZ=20.0; [cm]

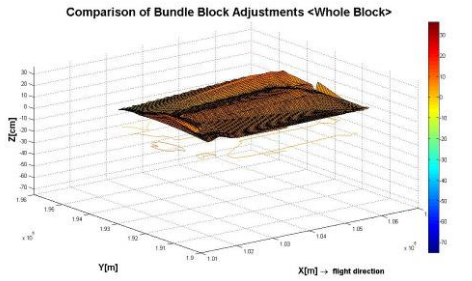

(b) RMSX=1.3, RMSY=1.5, RMSZ=10.7; [cm]

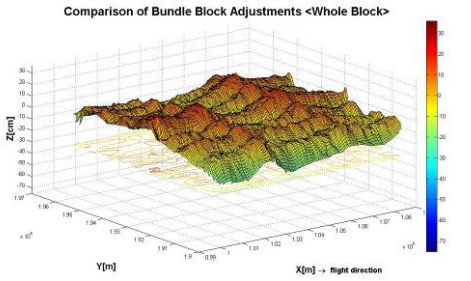

(c) RMSX=0.7, RMSY=0.9, RMSZ=7.2; [cm]

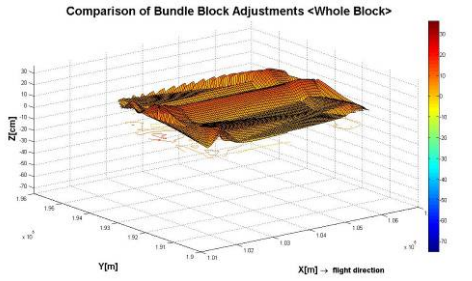

(d) RMSX=0.9, RMSY=1.2, RMSZ=8.3; [cm]

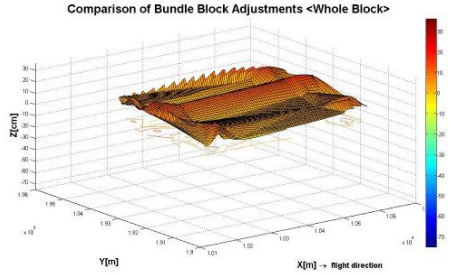

(e) RMSX=0.9, RMSY=1.2, RMSZ=7.5; [cm]

Figure 4.4.5-5, comparison of block adjustments – block Gent: (a) 80% side lap, no self-calibration against 20% side lap, no self-calibration; (b) 20% side lap: no self-calibration –- with GPS-data, no self-calibration,; (c) 20% side lap: no self-calibration –- parameters 1-12; (d) 20% side lap: no self-calibration –- parameters 1-12 and 30-41,74-77; (e) 20% side lap: no self-calibration –- parameters 1-12 and78, 80.

[scale range: -75cm up to 35cm]

Caused by the higher number of images per point also the effect of the systematic image errors to the ground position can be reduced. It seems that different to the figure 4.4.5-5-a that the difference of block adjustments of the sub-block Gent_20% with 60% end lap, 20% side lap and block Gent with 60% end lap, 80% side lap is very similar to the effect of additional parameters shown in figures 4.4.5-2 and 4.4.5-3.

The more stable block geometry makes the systematic effects stronger, so the block bending is more serious in the block Gent with higher overlap. The influence of the systematic effects can partly be compensated by control points. By theGent_20% the 0.9 GSD of RMSZ at check points was obtained in the block adjustments without self-calibration, the block adjustment with self-calibration or supported by GPS-data were not able to improve the accuracy of ground coordinates, the RMSZ of independent check points is in the range of 7 cm, corresponding 0.9 GSD. This indicates that the systematic image errors have only limited influence on the standard block with enough well-distributed high accurate control points.

Figure 4.4.5-6 shows the distribution of the object points in the whole UltraCam-block Istanbul. The block Istanbul is a small scale block; because of smaller overlap and much smaller number of tie points the geometry of the block is not so stable as the DMC-blocks Gent and Rubi.

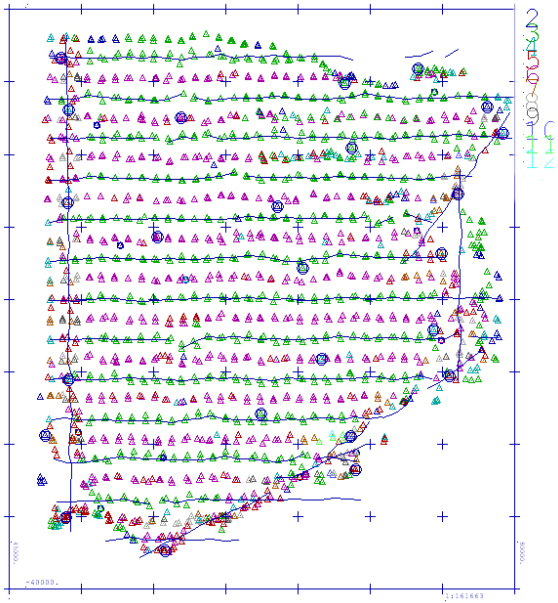

Figure 4.4.5-6: distribution of object points in the block Istanbul, color coded number of image per point.

The block deformation of UltraCamD-block Istanbul is shown in figure 4.4.5-7 through comparison of bundle block adjustments of all images in the block. The largest root mean square differences in Z (RMSZ) in the comparison of the block

adjustment without self-calibration and the block adjustment with standard parameters plus special UltraCam-parameters amounts to 114 cm, corresponding to 3.6 GSD. The block deformation of UltraCamD-block Istanbul is obviously much larger than for DMC-blocks Gent and Rubi. The root mean square differences in Z (RMSZ) of the whole block adjustment of the UltraCamD-block Istanbul cannot be compared directly with the DMC-blocks Gent and Rubi, because of the different block size, configuration, GSD and the distribution of control points. In general there is a stronger influence of the UltraCamD image deformation to the X- and Y-coordinates and a larger difference of the results with self-calibration just with the standard parameters 1-12 to the standard parameters plus the special UltraCam-parameters 42-73.

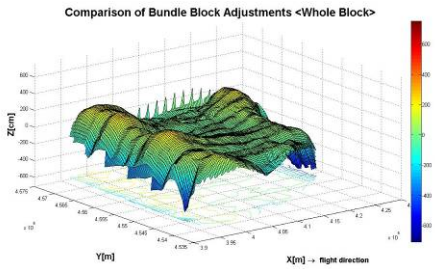

(a) RMSX=23.1, RMSY=29.0, RMSZ=116.2; [cm]

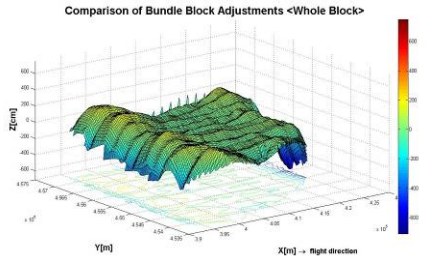

(b) RMSX=6.0, RMSY=8.4, RMSZ=105.1; [cm]

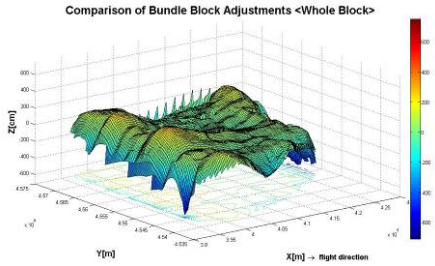

(c) RMSX=20.1, RMSY=27.6, RMSZ=113.9; [cm]

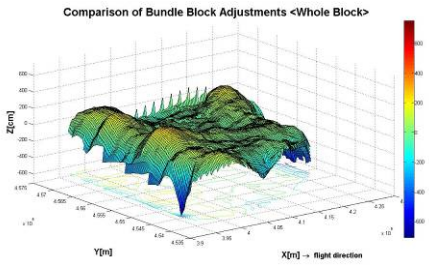

(c) RMSX=20.3, RMSY=25.1, RMSZ=113.8;[cm]

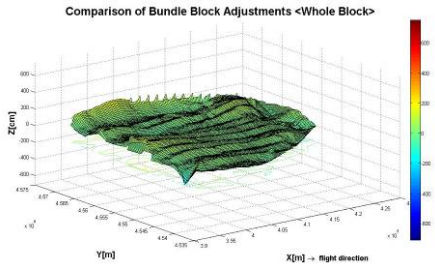

(e) RMSX=20.7, RMSY=23.3, RMSZ=47.0;[cm]

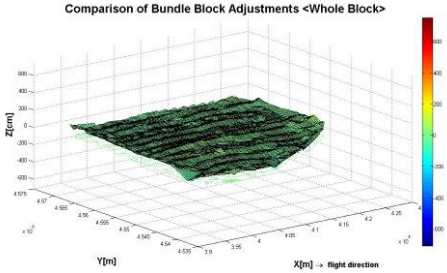

(f) RMSX=5.9, RMSY=7.0, RMSZ=22.6;[cm]

Figure 4.4.5-7, comparison of bundle block adjustments – UltraCamD-block Istanbul: (a) no self-calibration –against parameters 1-12; (b) no self-calibration –- parameter 9; (c) no self-calibration –- parameters 9 plus 42-73; (d) no self-calibration –- parameters 1-12 plus 42-73; (e) parameter 9–- parameters 1-12; (f) parameters1-12 –- parameter 1-12 plus 42-73. ***[scale range: -650cm up to 650cm]***

4.5.2 BLUH vs. MATCH-AT

The comparison of the two program systems BLUH and MATCH-AT shows some interesting results in the comparison of the achieved ground coordinates. The Grün parameters have a similar influence like the BLUH-parameters on the image deformation. The adjusted object points have systematic differences achieved by both programs. It seems that in MATCH-AT the image deformation is causing larger block deformations like with BLUH.

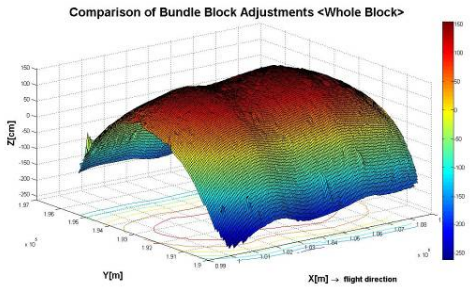

(a) RMSX=2.2, RMSY=2.7, RMSZ=101.0; [cm]

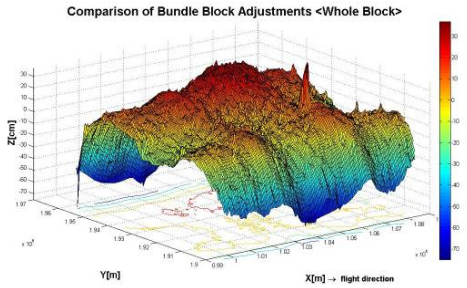

(b) [RMSX=1.9, RMSY=2.6, RMSZ=20.8; [cm]

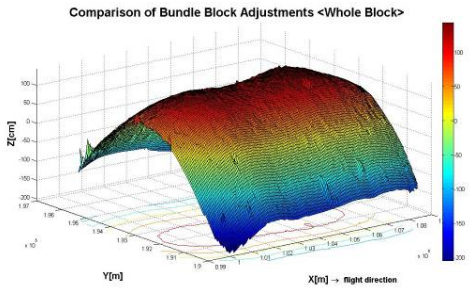

(c) RMSX=2.4, RMSY=3.5, RMSZ=85.1; [cm]

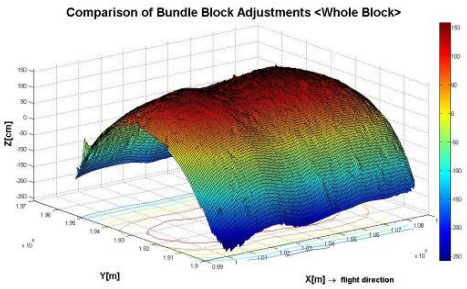

(d) RMSX=2.7, RMSY=3.0, RMSZ=103.9; [cm]

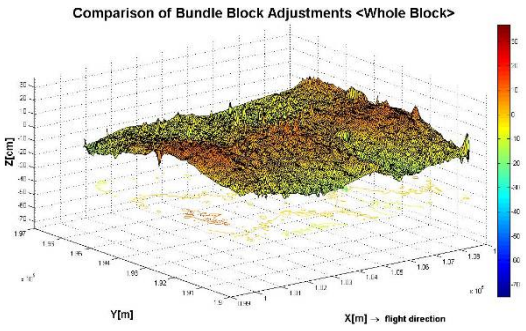

(e) RMSX=1.6, RMSY=2.6, RMSZ=5.5 [cm]

Figure 4.4.5-8, comparison of block adjustments between Match-AT and BLUH: (a) Match-AT, no self-calibration –against Match-AT, with Grün parameters; (b) BLUH, no self-calibration –- Match-AT, with Grün parameters; (c) Match-AT, no self-calibration –- BLUH, no self-calibration; (d) Match-AT, no self-calibration –- BLUH, parameters 1-12; (e) Match-AT, with Grün parameters –- BLUH, parameters 1-12.
(a), (c), (d) [scale range: -250cm up to 150cm]; (b), (e) [scale range: -75cm up to 35cm]

4.5.3 Model Deformation

The bundle block adjustment with self-calibration is not a problem; this can be handled like for analogue photos. The problem appears with the handling of stereo models. For the handling of stereo models usually systematic image errors are ignored, even if there is a strong influence to the height. For a horizontal mapping the systematic image errors can be ignored for analogue like for the large frame digital cameras. This is obvious by the shown accuracy range – the standard deviation in X and Y is not so much influenced by the systematic image errors respectively the self-calibration.

$$S_Z = Spx \cdot mb \cdot \frac{h}{b} \qquad (4.4.5\text{-}1)$$

With:

Sz: standard deviation of Z
Spx: standard deviation of x-parallax
mb: image scale
h: height above ground
b: base

The standard deviation of the x-parallax empirically is in the same range like σo. The formula 4.4.5-1 shows the dependency of the expected vertical accuracy of stereo measurement. If the standard deviation of the x-parallax Spx corresponds to the accuracy of the image coordinates, the vertical accuracy corresponds to the accuracy in X and Y multiplied with the height to base relation.

The influence of the model deformation caused by systematic image errors in the DMC-block Gent is shown in figure 4.4.5-9. The image model is based on the images 1001 and 1002 of block Gent with 60% end lap corresponding to the height to base relation 3.26. According to the formula 4.4.5-1 the expected vertical accuracy of well defined points is approximately 0.5 GSD.

The shown model deformation is based on image coordinates corrected by the corresponding systematic image errors and corresponding optimal orientation, only the relative effects play a roll. The model deformation based on the standard parameters 1-12 shows some general systematic effects as analogue photos, and the model deformation based on the special DMC-parameters shows some systematic effects caused by the merging of sub-images. The Z-discrepancy of the model deformation is in the range 0.2 GSD up to 0.4 GSD in accordance with different parameters. This is much better than for analogue photos; but in relation to the expected vertical accuracy it is not negligible.

In comparison of object points in stereo models based on the different adjustments, it shows interesting results that the special additional parameters for DMC have only a limited influence to the object coordinates, the results based on the standard parameters 1-12 and the results based on the standard parameters plus the special DMC parameters are not too different. Within the model the effect to the horizontal coordinate components is nearly negligible.

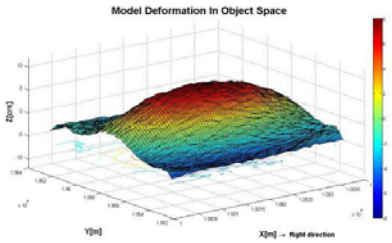

(a) RMSX=0.3, RMSY=0.4, RMSZ=3.4 [cm]

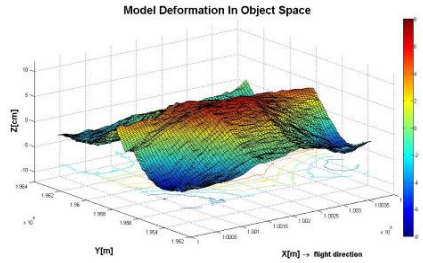

(b) RMSX=0.4, RMSY=1.1, RMSZ=3.0

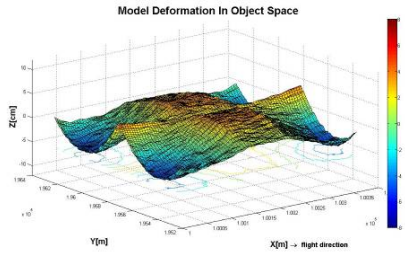

(c) RMSX=0.2, RMSY=1.0, RMSZ=1.7

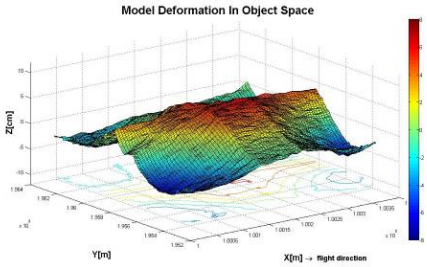

(d) RMSX=0.4, RMSY=1.1, RMSZ=3.0

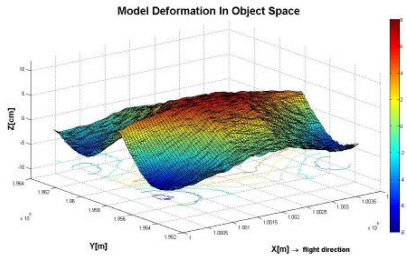

(e) RMSX=0.4, RMSY=1.1, RMSZ=3.2

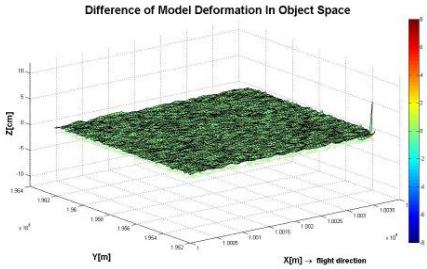

(f) RMSX=0.1, RMSY=0.2, RMSZ=0.2

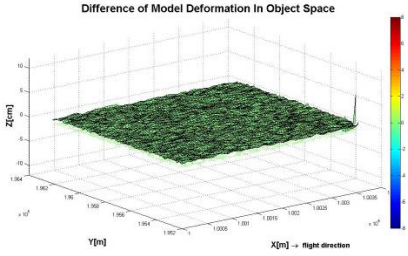

(g) RMSX=0.1, RMSY=0.1, RMSZ=0.2

Figure 4.4.5-9, influence of model deformation block Gent: (a) standard parameters 1-12; (b) DMC-parameters 30-41, 74-77; (c) DMC-parameters78, 80; (d) parameters 1-12 plus 30-41, 74-77; (e) parameters 1-12 plus 78, 80.
comparison of object points in stereo model based on different block adjustments :(f) parameters 1-12 against parameters 1-12 plus 30-41, 74-77; (g) parameters 1-12 against parameters 1-12 plus78, 80. ***[scale range: -8cm up to 8cm]***

Figure 4.4.5-10 shows the model deformation of sub-block Gent with 20% side lap. Based on the same image the deformation of sub-block Gent is a little smaller.

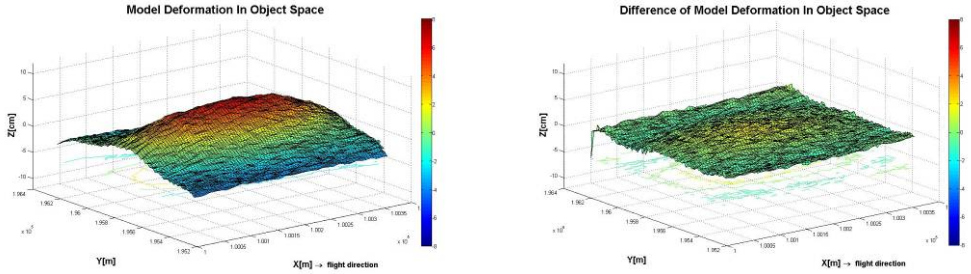

Figure 4.4.5-10: influence of model deformation sub-block Gent_20% with 20% side lap: (a) standard parameters 1-12; (b) difference of model deformation between block Gent with 80% side lap against sub-block Gent_20% based on parameters 1-12. ***[scale range: -8cm up to 8cm]***

The model used in figure 4.4.5-11 is based on the images 150047 and 150048 of UltraCamD-block Istanbul, with a height to base relation of 3.8. According to the formula 4.4.5-1 the expected accuracy is 38cm, corresponding to 1.2 GSD. The model deformation based on the different image corrections is causing Z-discrepancy of 0.6 up to 0.7 GSD. The influence to the height is more complex and local for the UltraCamD, while it is smoother for the DMC.

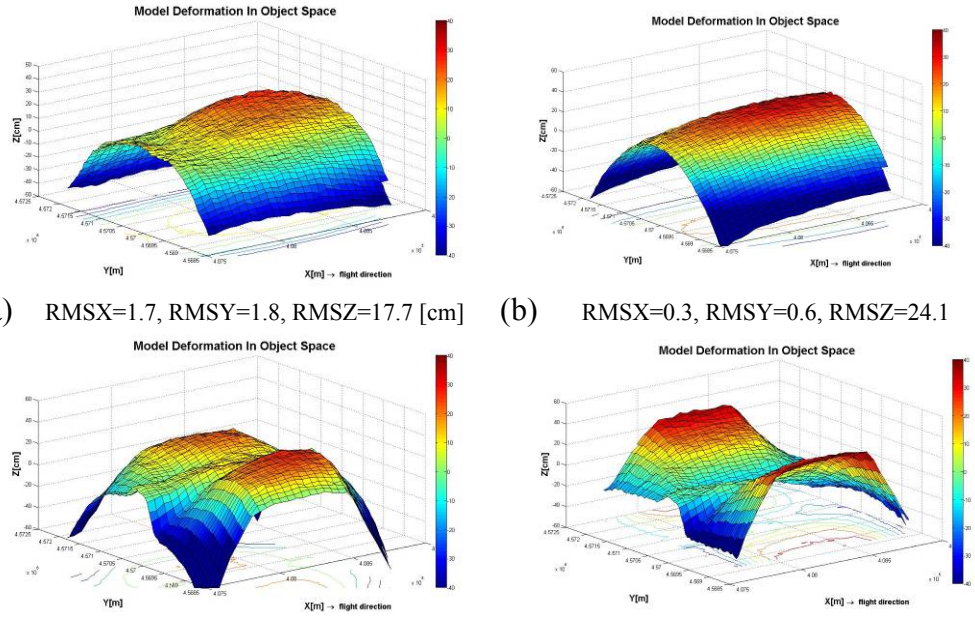

(a) RMSX=1.7, RMSY=1.8, RMSZ=17.7 [cm] (b) RMSX=0.3, RMSY=0.6, RMSZ=24.1

(c) RMSX=3.0, RMSY=7.3, RMSZ=21.1 (d) RMSX=2.8, RMSY=7.6, RMSZ=19.5

Figure 4.4.5-11: influence of model deformation: (a) standard parameters 1-12; (b) parameter 9; (c) parameter 9 plus UltraCam-parameters 42-73; (d) parameters 1-12 plus UltraCam-parameters 42-73. ***[scale range: -40cm up to 40cm]***

Usual commercial Digital Photogrammetric Workstation cannot respect the systematic image errors, so the generated object coordinates are influenced by the model deformation. The influence of the model deformation cannot be accepted for DEMs, by this reason the program DEMCOR for a posterior height correction of DEMs has been developed by the Leibniz University Hannover solving the problem of the model deformation. Another possibility is change of the image geometry by the systematic image errors with IMGEO. [Jacobsen, 2007]

Chapter
5. Conclusion

The investigation has proven clearly that the large frame digital cameras Intergraph DMC and Microsoft Photogrammetry UltraCamD have systematic image errors. Even with this limitation the high accuracy potential of digital frame cameras has been confirmed by the bundle block adjustments with DMC-images and UltraCamD-images leading to standard deviations of unit weight (σ_0) of 2µm and 3.5µm, corresponding 0.16 pixels and 0.38 pixels. This is quite better than for analogue photos. For check points standard deviations for X and Y of 0.3 GSD with the DMC and 0.7 GSD with UltraCam have been reached under operational conditions. It must be mentioned, that the analysis of UltraCamD-block Istanbul was limited by the accuracy of the available control points, so the full accuracy potential could not been tested. But in general a high accuracy level could be reached with the digital images.

For reaching the best accuracy, a combination of standard additional parameters used also for analogue photos and special parameters for the camera type should be used. The major part of the systematic image errors can be determined and respected with the standard set of additional parameters, the special parameters are only improving the result slightly. Based on the investigation of block Gent and Rubi, the geometry of DMC-image is quite stable, only very limited influenced by the systematic image errors, the self-calibration is not necessary, if the block adjustments are supported by high precise GPS-data or with enough well-distributed high precise control points.

The systematic image errors are causing not negligible model deformation in the vertical coordinate component. The influence to X and Y are negligible for the DMC and tolerable small for the UltraCamD caused by the more local character of the systematic image errors for UltraCamD. Since most commercial photogrammetric workstations are not able to respect systematic image errors, digital elevation models based on automatic image matching have to be improved a posterior by the effect of the systematic image errors like with the Hannover program DEMCOR. Of cause a quite better and more flexible solution would be the on-line use of systematic image

errors in photogrammetric work stations. With IMGEO also a program for the geometric change of the images based on the systematic image errors has been created solving the problems in the photogrammetric workstations.

Intergraph und Microsoft Photogrammetry are just working in improved calibration methods, so the described problems may be reduced in near future.

List of Formulae

List of Tables

List of Figures

Reference

Baz, I., Jacobsen, K., Büyüksalih, G., 2006: Analysis of a bundle block adjustment with UltraCamD images over Istanbul, Turkish-German Geodetic Days, Berlin 2006.

Baz, I., Buyuksalih, G., Jacobsen, K., 2007: Bundle Block Adjustment with High Resolution UltraCamD, ISPRS Hannover Workshop 2007

Diener, S., Kiefner, M., Dörstel, C. (2000):Radiometric normalisation and colour generation of the DMC. IAPRS Vol. XXXIII, Part B1, Amsterdam

DMC (2004): Z/Imaging (ed.): Specification Sheet: Digital Mapping Camera System

DMC (2005): Z/Imaging (ed.): User's Guide.

DMC (2006): Z/Imaging (ed.): Post-processing System User's Guide

Dörstel, C., Jacobsen, K., Zeidler, W. (2002): Geometric calibration of the DMC: Method and results. IAPRS (34), Part I Com I, pp 324-333. Denver.

Dörstel, C., Jacobsen, K., Stallman, D. (2003): DMC-Photogrammetric accuracy – Calibration aspects and generation of synthetic DMC images. In Grün/Kahmen (sds.): Proceedings on Optical 3D Measurement techniques VI, Zürich, Switzerland, pp. 74-82.

Ebner, H. (1976): Self Calibration Block Adjustment. ISP Congress XIII, Com. III, Helsinki, 17 pages.

Faugeras, O., Fua, P., Hotz, B., Ma, R., Robert, L., Thonnat, M., and Zhang, Z. (1992): Quantitative and Qualitative Comparison of some Area and Feature-Based Stereo

Algorithms. In Förstner, W. and Ruwiedl, S., editors, *Robust Computer Vision*, pages 1-26, Karlsruhe, Germany. Wichmann.

Grün, A. (1978): Progress in Photogrammetric Point Determination by Compensation of Systematic Errors and Detection of Gross Errors. International Society for Photogrammetry, Symposium of Commission III, Moscow, USSR

Hinz, A. (1999): The Z/I Imaging digital aerial camera system. In: Proceedings of the 47th Photogrammetric Week. Stuttgart, pp-203-214

Hinz A., Dörstel C, Heier H. (2001): DMC – The Digital Sensor Technology of Z/IImaging, Photogrammetric Week 2001, Eds D. Fritsch / R. Spiller, Wichmann, Heidelberg pp 93 - 103.

Jacobsen, K. (1982): Programmgesteuerte Auswahl zusätzlicher Parameter. In BuL 1982, 213-217

Jacobsen K. (1998): Development of Program System BLUH for bundle block adjustment in the University of Hannover, Festschrift Gottfried Konecny, Wissenschaftliche Arbeiten der Fachrichtung Vermessungswesen der Universität Hannover, Nr. 227, pp.157-162.

Jacobsen, K. (2004): Direct integrated sensor orientation — pros and cons. International Archives of Photogrammetry, Remote Sensing and Spatial Information Sciences 35 (Part B3), 829–835.

Jacobsen, K. (2007a): User Manual, BLIM

Jacobsen, K. (2006b): User Manual, BLUH

Jacobsen, K. (2007): Geometry and Information Contents of Large Size Digital Frame Cameras, ISPRS Hannover Workshop 2007

Jacobsen K. (2007): "Geometry of Digital Frame Cameras". In: Proceedings of ASPRS 2007 Annual Conference, Tampa, Florida, USA, May 7-11, 2007.On CD-ROM.

Jacobsen, K., (2006): Geometrische Analyse der Intergraph DMC. Internal report, not published

Klaus, A.; Bauer, J.; Karner, K.; Elbischger, P.; Perko, R.; Bischof, H. (2004): Computer Vision and Pattern Recognition, 2004. CVPR 2004. Proceedings of the 2004 IEEE Computer Society Conference onVolume 1, Issue , 27 June-2 July 2004 Page(s): I-151 - I-157 Vol.1

Kröpfl, M., Kruck, E., and Gruber, M. (2004a): Geometric calibration of the digital large format aerial camera UltraCamD. ISPRS Commission III: Theory and Algorithms.

Kröpfl, M., Kruck, E., and Gruber, M. (2004b): Introduction of the 3-DAS-1 digital aerial scanner. ISPRS Commission I: Sensors, Platforms and Imagery.

Leberl, F., Perko, R., Gruber, M., and Ponticelli, M. (2002b): Novel concepts for aerial digital cameras. ISPRS Commission I: Sensors, Platforms and Imagery.

Leberl, F., Gruber, M., Ponticelli, M., Bern¨ogger, S., and Perko, R. (2003): The UltraCam large format aerial digital camera system, Proceedings of the American Society for Photogrammetry & Remote Sensing, Anchorage, Alaska.

Madani, M. ; Dörstel, C. ; Heipke, C. ; Jacobsen, K.: DMC Practical Experience and Accuracy Assessment: IntArchPhRS. Band XXXV, Teil B2. Istanbul, 2004, S. 396-401

Shortis M & Beyer H (1996): Sensor technology for close range photogrammetry and machine vision, in Atkinson K (ed) Close Range Photogrammetry and Machine Vision, 1st Edition 371, United Kingdom: Whittles Publishing. ISBN 1 870325 46 X

Spreckels, V., Schlienkamp, A., Jacobsen, K., 2007: - Model Deformation – Accuracy of Digital Frame Cameras, ISPRS Hannover Workshop 2007

Tang, L., Dörstel, C., Jacobsen, K., Heipke, C., Hinz, A. (2000): Geometric accuracy potential of the Digtal Modular Camera. IAPRS, Vol. XXXIII, Part B4, Amsterdam

Vexcel Imaging Austria (2003): Announcing the UltraCamD. http://www.vexcel.co.at/downloads/UCD-announcement-May2003.pdf.